9-21-2022

Cardiovascular positron emission tomography: established and emerging role in cardiovascular diseases

Amit Bansal

Karthikeyan Ananthasubramaniam
Henry Ford Health, kananth1@hfhs.org

Recommended Citation
Bansal A, and Ananthasubramaniam K. Cardiovascular positron emission tomography: established and emerging role in cardiovascular diseases. Heart Fail Rev 2022.

Heart Failure Reviews
https://doi.org/10.1007/s10741-022-10270-6

Cardiovascular positron emission tomography: established and emerging role in cardiovascular diseases

Amit Bansal[1] · **Karthikeyan Ananthasubramaniam**[2]

Accepted: 4 September 2022

Abstract
Cardiac positron emission tomography (PET) imaging has established themselves firmly as excellent and reliable functional imaging modalities in assessment of the spectrum of coronary artery disease. With the explosion of technology advances and the dream of flow quantification now a reality, the value of PET is now well realized. Cardiac PET has proved itself as precise imaging modality that provides functional imaging of the heart in addition to anatomical imaging. It has established itself as one of the best available techniques for evaluation of myocardial viability. Hybrid PET/computed tomography provides simultaneous integration of coronary anatomy and function with myocardial perfusion and metabolism, thereby improving characterization of the dysfunctional area and chronic coronary artery disease. The availability of quantitative myocardial blood flow evaluation with PET provides additional prognostic information and increases diagnostic accuracy in the management of patients with coronary artery disease. Hybrid imaging seems to hold immense potential in optimizing management of cardiovascular diseases and furthering clinical research.

Keywords Positron emission tomography · Coronary artery disease · Myocardial viability · Microvascular dysfunction · Sarcoidosis · Prosthetic valve · Device infection

Overview of positron emission tomography and physics fundamentals

Since the initial clinical usage of positron emission tomography (PET), which started more than 40 years ago [1], PET has been used for noninvasive evaluation and monitoring of various cardiac conditions [2]. Cardiac PET allows not only functional but also detailed metabolic evaluation of the heart, which is unique compared to other cardiovascular imaging techniques like echocardiography or cardiac computed tomographic angiography that primarily provide anatomical imaging [3]. It is a highly sensitive imaging technique that can measure the physiologic process of metabolism, blood flow, inflammatory, or neoplastic activity occurring in the body for which a targeted radiotracer is available. After the radiotracer is injected into the body, it accumulates in the areas of active disease and resulting images are then typically combined with an anatomic imaging modality such as computed tomography (CT) or more recently magnetic resonance (MR), which enables co-registration and anatomic localization [4]. Combined PET/CT or PET/MR allows simultaneous imaging of anatomy from CT/cardiac magnetic resonance (CMR) and physiology from PET. PET is established as one of the best available tests for the assessment of myocardial tissue viability as well as for the evaluation of myocardial perfusion and is the current gold standard for noninvasive estimation of coronary flow reserve [5, 6]. The high spatial resolution (4 mm) of PET makes it more sensitive and specific as compared to other nuclear imaging techniques [7] .

PET imaging is based on positron emission by a decaying radionuclide. A positron is equivalent to an electron with the same mass but opposite electrical charge. Positrons are released from a proton inside the nucleus to collide with electrons orbiting around the nucleus. When a positron collides with an electron, it leads to annihilation reaction, forming a pair of 511-keV gamma-ray photons traveling in opposite directions [7]. PET imaging allows detection of radionuclide-labeled tracer accumulation in tissues with

✉ Karthikeyan Ananthasubramaniam
kananth1@hfhs.org

[1] UHS Wilson Medical Center, Johnson City, NY, USA

[2] Heart and Vascular Institute, Henry Ford West Bloomfield Hospital, 6777 W Maple, West Bloomfield, MI 48322, USA

Published online: 21 September 2022

high sensitivity and provides precise quantification of their local concentration (Table 1) [8].

Overview of PET isotopes

Various radiotracers used for cardiac PET imaging are summarized as follows.

Radiotracers for myocardial perfusion imaging

PET radiotracers for evaluation of myocardial blood flow (MBF) include well-established tracers, such as ^{15}O-labeled water (^{15}O-H2O), [9] ^{13}N-labeled ammonia (^{13}NH3) [10], and ^{82}Rubidium (^{82}Rb) [11], and newer tracers like ^{18}F-Flurpiridaz, which has been validated in animals [12] and humans [13], and is now being further evaluated in phase 3 trials. ^{15}O-H2O is generated by a cyclotron (half-life 2 min) and is considered the most ideal perfusion tracer because of its physiological properties. It is freely diffusible and has a high first-pass extraction of 95%. Its uptake is nearly linear with no roll-off in extraction at higher coronary flows, which results in underestimation of MBF [14]. However, because of its short half-life seconds, need for onsite cyclotron, poor tissue accumulation, and challenges with image quality, it is primarily used for research.

$^{13}NH_3$ also requires cyclotron for production (half-life 9.9 min) and is considered the preferred tracer among the available perfusion tracers because of its superior physical properties and pharmacokinetics. $^{13}NH_3$ enters the myocardium either as NH_3 or through Na+/K+-ATPase as NH_4+. The tracer is then converted and trapped intracellularly as ^{13} N-glutamine. This results in a very high extraction fraction of about 80% at baseline MBF, which decreases nonlinearly with increasing flows due to roll-off [15] $^{13}NH_3$ produces high-quality images with excellent resolution because of its long half-life of 9.96 min and short mean positron path length. Exercise stress PET is feasible with $^{13}NH_3$.

^{82}Rb is made from strontium-82 (^{82}Sr) using a ^{82}Sr/^{82}Rb generator. Na+/K+-ATPase facilitates the uptake of ^{82}Rb into the myocardium. ^{82}Rb has a lower first-pass extraction fraction of 60% at baseline MBF, but at high flows it is affected by greater roll-off [15]. Despite this, studies have shown reliable MBF quantification with ^{82}Rb. ^{82}Rb has longer mean positron range, which attributes to its lower spatial resolution and degradation in image quality [16]. One of the very important advantages of ^{82}Rb is it does not require onsite cyclotron, making it the most widely used PET flow tracer in clinical use in the USA. Also, ^{82}Rb's ultrashort half-life of 76 s allows for rapid sequential perfusion imaging, although exercise-based testing is not currently practical or feasible [17].

^{18}F-Flurpiridaz is a newer radiotracer that has been studied widely in animals [18]. It has a longer half-life (110 min), high myocardial extraction fraction independent of flow, excellent spatial resolution, and short mean positron range, which allows for high image resolution. ^{18}F-Flurpiridaz can be acquired and transported from regional cyclotrons and may open the doors of exercise PET imaging given its longer half-life. It is currently being evaluated in phase 3 trials and hopefully will enter the clinical arena in the near future. Table 2 highlights the key clinical characteristics of perfusion radiotracers.

^{11}C-Acetate is a PET radiotracer primarily delegated to study oxidative metabolism and is limited to centers with cyclotron capabilities and research applications.

Radiotracers for myocardial metabolism, viability, and inflammation/infection

^{18}F-Fluorodeoxyglucose (FDG) is the most commonly used radiotracer for assessing myocardial viability, metabolic activity, and inflammation/infection. A glucose analog, deoxyglucose, is coupled with the tracer ^{18}F, which enters cardiomyocytes using glucose transporters. It then gets phosphorylated by hexokinase into ^{18}F-FDG-6-phosphate. Unlike glucose, FDG gets trapped inside the cell and does not undergo further metabolism [19]. FDG uptake is increased in chronically underperfused but viable myocardium (hibernating myocardium) because of preferential utilization of

Table 1 Some key differences in cardiac PET vs SPECT imaging

	PET	SPECT
Type of stress feasible	Predominantly pharmacologic	Exercise or pharmacologic
Isotope ENERGY for clinical use	511 keV	65–140 keV
Attenuation correction	Routine	Optional
Sensitivity and resolution	Higher	Lower
Flexibility of incorporating isotopes into biomolecules	Routine	Challenging
Cost	More	Less
Blood flow and flow reserve assessment	Well established	Limited availability

Table 2 Comparison of key properties of cardiac PET perfusion tracers

	^{15}O-Water	^{13} N-Ammonia	^{82}Rubidium	^{18}F-Flurpiridaz
Positron range, mm	4.14	2.53	8.6	1.03
Half-life, minutes	2.07	9.96	1.25	110
Myocardial extraction fraction	100%	80%	60–65%	94%
Image resolution	Intermediate	Intermediate-high	Lowest	Highest
Production	On-site cyclotron	On-site or nearby cyclotron	^{82}Sr/^{82}Rb generator	Regional cyclotron

^{82}Rb ^{82}Rubidium, *^{82}Sr* strontium-82, *PET* positron emission tomography

glucose by these cells. FDG uptake is decreased or even absent in myocardial scars. Because of the relatively long physical half-life of ^{18}F nuclide (approximately 120 min), it can be produced at a central location and distributed to smaller centers, thereby obviating the need of on-site cyclotron at smaller centers. Along the same lines, detection of areas of myocardial inflammation and infection using ^{18}F-FDG is being exploited for evaluating diseases like sarcoidosis, prosthetic valve, and cardiac device–based infections.

Newer PET radiotracers in pipeline

The most promising radiotracer developments include the application of existing tracers such as ^{18}F-NaF in atherosclerosis. Similarly, ^{18}F-based radiotracers for diagnosis of cardiac amyloidosis include ^{18}F-florbetaben, ^{18}F-florbetapir, and ^{18}F-flutemetamol. For cardiac sarcoidosis, ^{68} Ga-DOTA-conjugated peptide compounds—^{68} Ga-DOTATOC, ^{68} Ga-DOTATATE, and ^{68} Ga-DOTANOC—are quite promising as they have no physiological myocardial uptake. The ^{18}F-labeled sympathetic nerve PET radiotracer ^{18}F-LMI1195 (also known as ^{18}F-flubrobenguane) seems very promising with potential to aid clinical decision-making, e.g., for optimal selection of patients requiring an implantable cardioverter-defibrillator or cardiac resynchronization therapy [8].

Current clinical applications of cardiac PET

PET in coronary artery disease and microvascular dysfunction

PET is being increasingly used in the diagnosis of coronary artery disease (CAD) because of its high accuracy and ability to provide functional imaging of the heart as compared to other noninvasive imaging modalities that primarily provide anatomical imaging [20]. PET helps in the diagnosis, risk stratification, and prognostication of suspected or known CAD. Moreover, it is also helpful in diagnosing endothelial and microvascular dysfunction [2].

PET has emerged as a superior imaging technique as compared to widely used SPECT [21], because of its higher spatial resolution and ability to incorporate routine attenuation correction of images. PET comes with additional advantages of reduced radiation exposure, superior soft tissue contrast, motion and partial volume correction, and multiparametric multiorgan assessments [4]. A normal cardiac PET is characterized by homogenous distribution of radiotracer and normal perfusion (Fig. 1), normal gated wall motion, and ejection fraction (EF) with normal stress electrocardiographic response. PET myocardial perfusion imaging (MPI) has a high sensitivity of 92% and high specificity of 85% in diagnosing CAD for stenosis > 50% in diameter seen on invasive coronary angiography, as shown in case example (Fig. 2). The high specificity of PET is due to the reduced number of artifacts related to photon attenuation leading to less false positives. PET cardiac stress imaging is also associated with lower radiation compared to SPECT.

A significant advantage of PET over SPECT is its ability to assess absolute MBF in milliliters per gram per minute and ability to estimate coronary or myocardial flow reserve (MFR) [22, 23]. Assessment of MBF by PET imaging provides a major boost to PET assessment of CAD and microvascular function by quantifying hyperemic or peak MBF (PMBF) [22, 24]. Normal resting blood flow is typically between 0.6 and 1.2 ml/min/g, and hyperemic or PMBF typically should be at least double of resting flow (or higher in younger age group where it is 3–4 times baseline flow). Values of ≥ 1.8 ml/min/gram of PMBF are typically not associated with obstructive epicardial CAD. Among patients with severe 3-vessel CAD, MFR is usually globally reduced and is an independent predictor of 3-vessel CAD. Patients with more severely reduced stress MBF and MFR are at higher CAD than patients with preserved values or modest reductions. Analysis of relationship between MFR and cardiac mortality suggests an excellent prognosis for MFR > 2 and a steady increase in cardiac mortality for an MFR < 2. Patients with severely decreased MFR < 1.5 are at much higher risk of CAD as compared to patients with reduced MFR < 1.8 or normal MFR greater than 2. Traditional evaluation by SPECT MPI [25] is not robust enough for flow quantification although new solid-state SPECT systems have enabled SPECT flow assessment to become a possibility, however still in its infancy compared to PET. Electrocardiogram

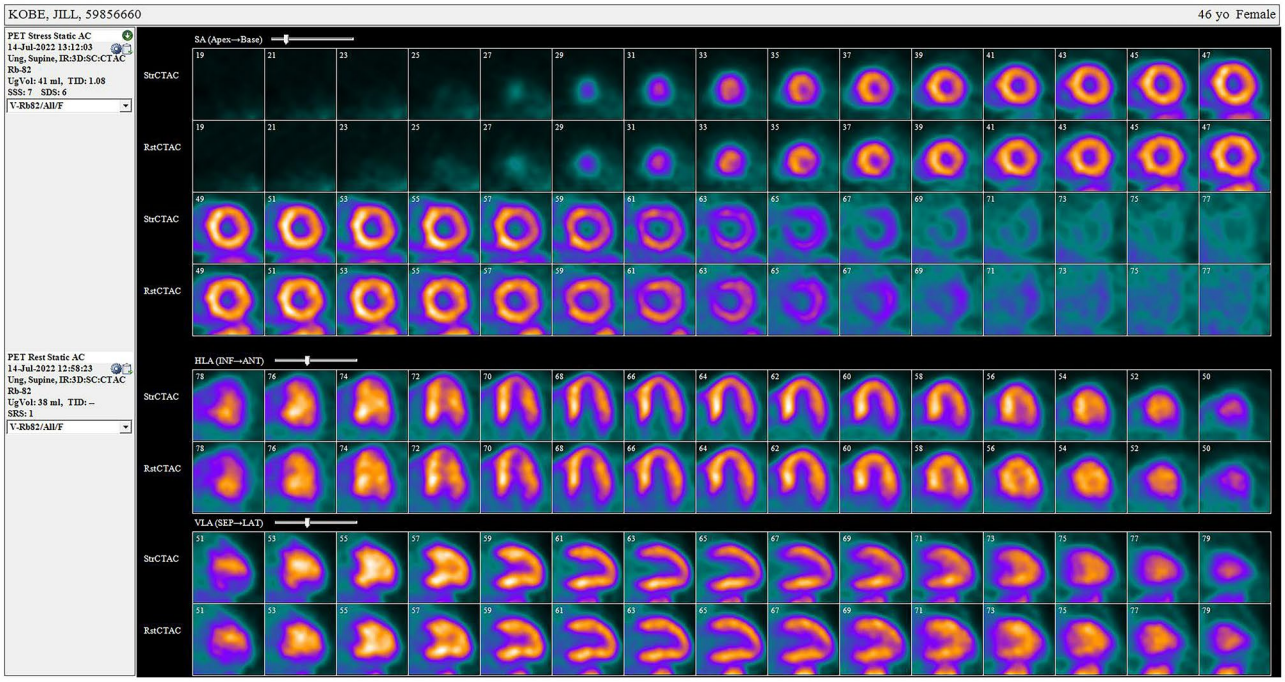

Fig. 1 A 72-year-old female with severe bilateral knee arthritis, diabetes, hyperlipidemia, and hypertension underwent ^{82}Rb PET regadenoson stress for preoperative risk assessment for carotid surgery. Rest and stress perfusion were normal and rest EF was 64% and peak stress EF was 68% and stress electrocardiogram was normal. Abbreviations: ^{82}Rb, Rubidium-82; ANT, anterior; CTAC, computed tomography–based attenuation correction; EF, ejection fraction; HLA, horizontal long axis; INF, inferior; LAD, left anterior descending artery; LAT, lateral; MBF, myocardial blood flow; MFR, myocardial flow reserve; PET, positron emission tomography; Rst, rest; SA, short axis; SEP, septal; SRS, summed rest score; SSS, summed stress score; Str, stress; VLA, vertical long axis

(ECG)-gated PET also has some unique advantages as it can be used to measure left ventricular EF (LVEF) at peak hyperemic stress (not done with SPECT) and enable calculation of EF reserve (peak stress EF − rest EF). In a normal healthy person, LVEF increases during peak vasodilator stress in PET, but in severe CAD (as in 3-vessel or significant left main disease) patients, it decreases from baseline to peak stress with or without worsening perfusion defects seen on stress [26]. Serial monitoring of changes in LVEF reserve can be used for risk stratification [27].

PMBF measurement by PET also helps in enhanced characterization of CAD burden and identification of balanced ischemia by detecting decreased MBF in all vascular territories, a situation where SPECT imaging has been shown to underestimate disease. In one study, SPECT imaging was found to detect only about 10% of patients with severe 3-vessel CAD or significant left main coronary artery stenosis of 50% or greater [28]. Addition of gated SPECT images can improve the identification of this subset to about 25% and thus still leaves substantial area of uncertainty. On the other hand, PET can identify the hemodynamically significant culprit lesion along with the true extent of ischemia in a multi-vessel territory in most cases [29]. Furthermore, diffuse reduction in PMBF and reduction in MFR in an otherwise normal or mildly abnormal scan with abnormal EF reserve are valuable adjunctive clues in PET to multi-vessel disease. Three examples of multi-vessel ischemia on ^{82}Rb stress PET perfusion are shown in Figs. 3–4. Furthermore, evaluating PMBF by PET (with a global marked blunted or flat response in PMBF) can provide insights into potential possibility of pharmacologic vasodilator non responsiveness with PET as a cause of non-diagnostic scan, which cannot be achieved with current SPECT technology. MBF and MFR are also the best current noninvasive method to evaluate the coronary microcirculation. Abnormalities of PMBF and MFR in the absence of significant epicardial CAD can help diagnose microvascular dysfunction. An example case is shown in Fig. 4. Abnormal MFR (< 2) has been found to be an independent prognostic factor of cardiac mortality regardless of presence or absence of epicardial CAD [30]. Thus, stress PET may be a valuable tool in assessment of patients with subjective or objective evidence for ischemia with no obstructive CAD on angiography for evaluation of microvascular disease. Cardiac PET can also evaluate endothelium-dependent vasoreactivity by using the cold pressor test, thereby providing an estimate of

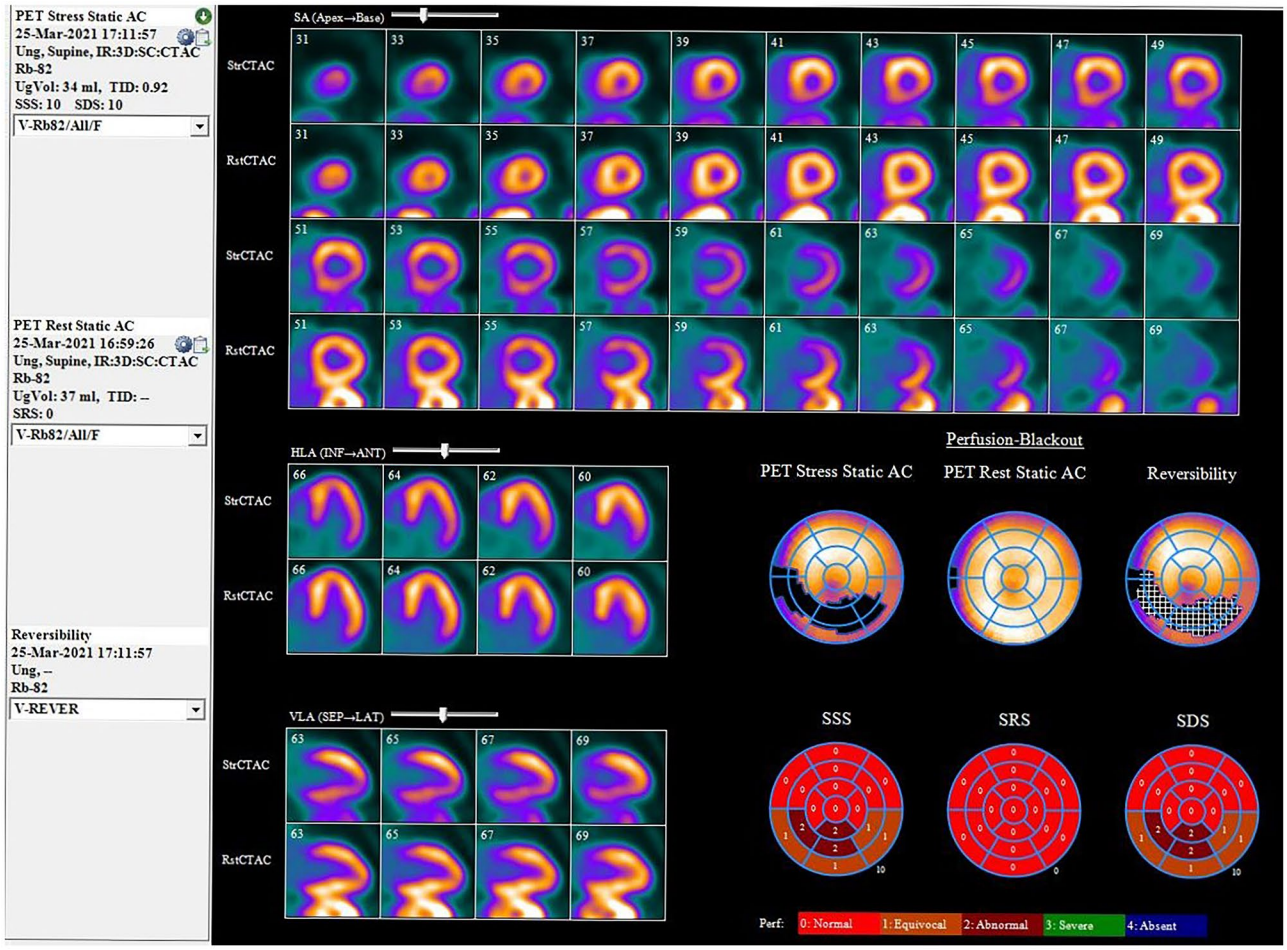

Fig. 2 A 70-year-old woman with chest discomfort undergoing Rb-82 stress PET showing reversible perfusion defect in the inferior inferolateral walls. Coronary angiography showed 80% stenosis in a dominant left circumflex artery. Abbreviations: ^{82}Rb, Rubidium-82; ANT, anterior; CTAC, computed tomography–based attenuation correction; HLA, horizontal long axis; INF, inferior; LAT, lateral; PET, positron emission tomography; Rst, rest; SA, short axis; SEP, septal; Str, stress; VLA, vertical long axis

endothelial integrity that can be compromised in patients with coronary risk factors [31], such as diabetes, hypertension, hypercholesterolemia, and smoking.

Hybrid PET/CT imaging allows simultaneous integration of coronary anatomy and function with myocardial perfusion and metabolism in a single examination, thereby improving better diagnostic accuracy [20, 32]. Estimation of calcium burden and score and combining coronary CT as indicated in patients with suspected CAD not only provide better definition of hemodynamic significance of coronary stenosis, but also refine long-term prognosis [33]. Fig. 5 is an example of PET/CT in a patient with extensive calcific burden but with normal perfusion. Thus, the complementary assessment of atherosclerosis with calcium evaluation and functional data with perfusion helps risk stratify patients for long-term aggressive risk reduction yet avoidance of any invasive workup given normal functional information. Such a decision can be further enhanced by concomitant evaluation of flow data, which can help rule out balanced ischemia.

PET in special patient populations with CAD

Left bundle branch block

In the Framingham study [34], CAD was found in 40% of patients with left bundle branch block (LBBB) and was associated with a fourfold increase in cardiovascular mortality. It is well recognized that evaluating patients with LBBB for CAD by stress echocardiography and SPECT is usually confounded by septal wall motion abnormalities and septal perfusion defects, respectively [35]. Various studies have found that septal defects on SPECT imaging can be seen in 4 to 53% of studies [36]. Proposed explanations for these septal defects include reduced septal blood flow due to cardiac

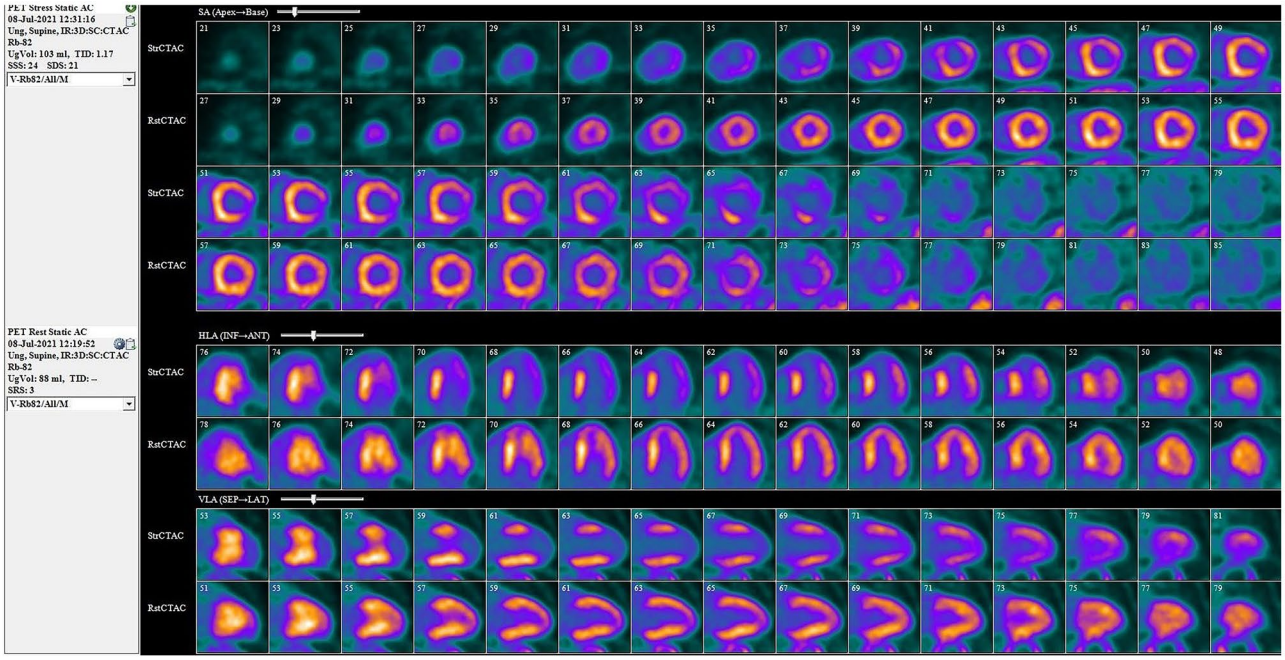

Fig. 3 A 70-year-old diabetic male with prior nondiagnostic SPECT from artifacts referred for vasodilator 82-Rb PET stress imaging. Perfusion images show a large area of reversible defects in the mid-distal septum and anterior anterolateral walls extending to apex suggesting LAD (left anterior descending artery) ischemia. Additional reversible inferolateral defect suggesting left circumflex ischemia. Gated rest EF was 46% and peak stress EF was 44%. Coronary angiography showed 60% left main, 80% LAD and 90% left circumflex disease. Abbreviations: ^{82}Rb, Rubidium-82; LAD, left anterior descending; PET, positron emission tomography; SPECT, single photon emission computed tomography. Abbreviations: ANT, anterior; CTAC, computed tomography-based attenuation correction; HLA, horizontal long axis; INF, inferior; LAT, lateral; Rst, rest; SA, short axis; SEP, septal; Str, stress; VLA, vertical long axis

dyssynchrony, partial volume effects, and septal microvascular dysfunction [37, 38]. PET stress MPI has emerged as a promising noninvasive imaging method for diagnosis and risk stratification of CAD. It has several advantages compared to SPECT MPI due to superior spatial resolution. In addition to assessing myocardial perfusion, left ventricular function, and wall motion, ^{82}Rb-PET can quantify global and regional MBF during both rest and stress and can also measure coronary flow reserve, providing further clarification on the true nature of observed septal defects [39, 40]. PET has been found to improve the diagnostic utility of MPI in patients with LBBB. In a study of 440 patients with LBBB undergoing MPI, 67 underwent PET imaging and 373 underwent SPECT imaging. Septal perfusion defects were found to be significantly less common with PET as compared to that with SPECT (1.5% vs 19.3%, $P<0.001$) [41]. Another study by Vidula et al. revealed that in detecting obstructive CAD, PET when compared to SPECT demonstrated higher sensitivity (88% vs 60%), specificity (56% vs 14%), positive predictive value (64% vs 20%), negative predictive value (83% vs 50%), and overall superior diagnostic accuracy (area under the curve 0.72 [95% CI 0.50–0.93] vs 0.37 [95% CI 0.20–0.54], $P=0.01$). LBBB/ventricular-paced rhythm-related septal and anteroseptal defects were significantly less with PET compared to SPECT (septal: 17% vs 72%, $P=0.001$; anteroseptal: 8% vs 47%, $P=0.02$) [42].

Obesity

The diagnosis of CAD and risk stratification in obese patients can be very challenging due to various limitations of commonly used imaging modalities in this population [43].

Stress echocardiography is limited by poor acoustic windows and is significantly dependent on the operator's experience. The use of echo enhancing agents improves endocardial definition and left ventricular opacification; however, the prognostic value of this technique is still uncertain in obese patients. Transesophageal dobutamine stress echocardiography can help overcome the issue of poor acoustic windows, but this is a semi-invasive modality. CT angiography and calcium score are often limited due to noisy images, need for strict heart rate control, and the continued inability to estimate physiologic significance of moderate anatomic stenosis in most centers [43]. Stress perfusion CMR is usually limited due to its cost and limited availability. Moreover, CMR cannot usually be performed in patients

a

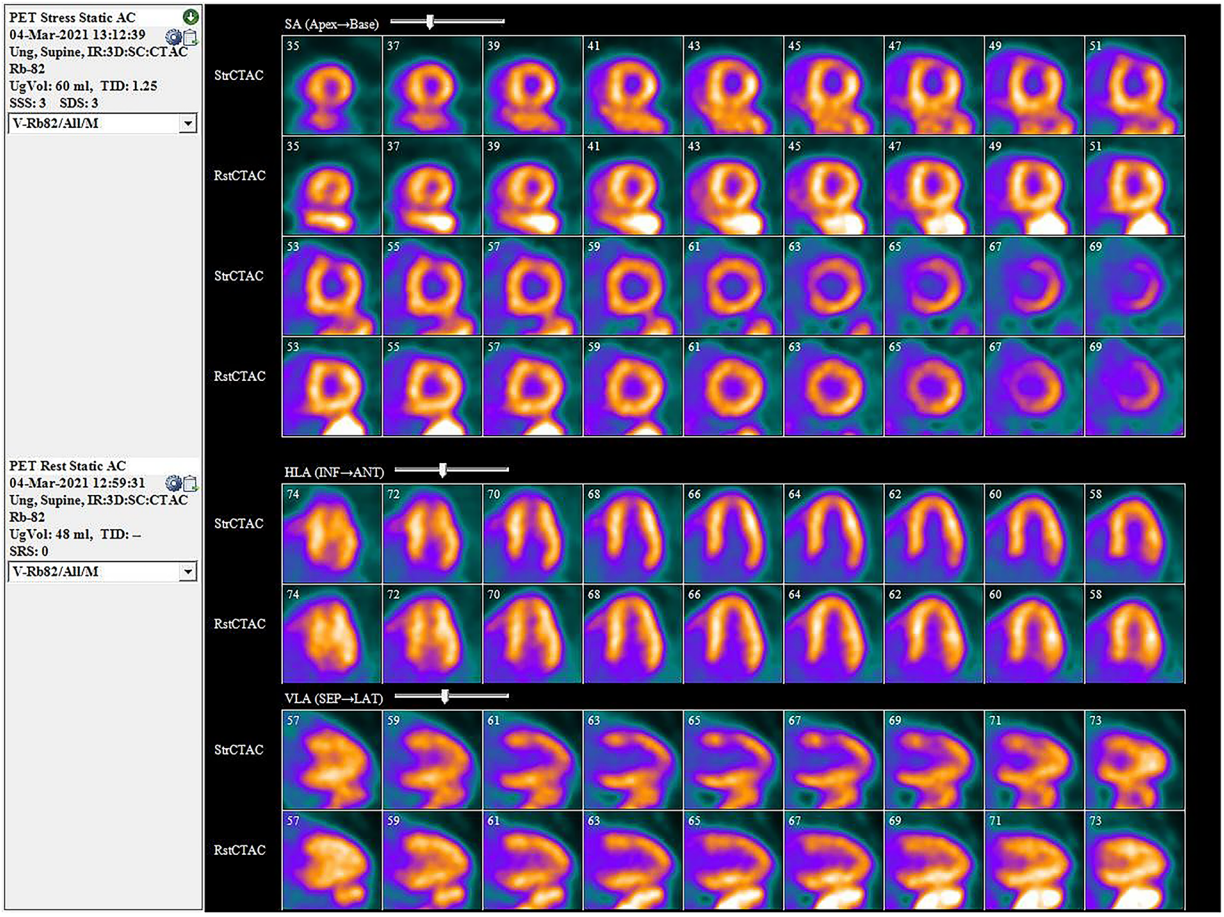

b

Global Results

Region	Mean MC Str	Mean MC Rst	Flow (ml/min/g) MC Str	Flow (ml/min/g) MC Rst	Reserve
LAD	77%	79%	1.44	1.10	1.32
LCX	87%	90%	1.60	1.25	1.28
RCA	89%	88%	1.95	1.17	1.67
TOT	83%	84%	1.63	1.16	1.41

Fig. 4 Perfusion PET images (**a**) show small anterior-apical wall reversible defect (top panel). Bottom panel flow analysis (**b**) shows diffuse severe reduction in PMBF (MC str) in all 3 coronary territories along with reduction in MFR globally. Gated stress EF was 56% and peak stress EF was unchanged at 56%. Patient underwent coronary angiography showing significant distal left main of 70% and 90% large diagonal stenosis and nondominant RCA disease. Abbreviations: ANT, anterior; CTAC, computed tomography–based attenuation correction; EF, ejection fraction; HLA, horizontal long axis; INF, inferior; LAD, left anterior descending artery; LAT, lateral; LCX, left circumflex artery; MFR, myocardial flow reserve; PET, positron emission tomography; PMBF, peak myocardial blood flow; RCA, right coronary artery; ROI, region of interest; Rst, rest; SA, short axis; SEP, septal; Str, stress; VLA, vertical long axis

with severe renal impairment and implanted devices and some obese patients cannot fit in the scanner console and are claustrophobic.

The use of SPECT MPI for evaluation of CAD in obese patients also has certain limitations including its susceptibility to attenuation in the absence of attenuation correction, photon scatter, and reduced signal-to-noise ratio [44]. Moreover, limited table load and gantry approach with diameter of the SPECT scanner limit its use in extremely obese patients [45].

PET provides better diagnostic accuracy than SPECT in obese patients as it has a higher spatial resolution (5–7 mm) as compared to SPECT (10–15 mm) [44]. In a meta-analysis of 3099 patients, Mc Ardle et al. found that for the diagnosis of obstructive CAD, PET had greater diagnostic accuracy than SPECT, with sensitivity of 90% and 85%, specificity

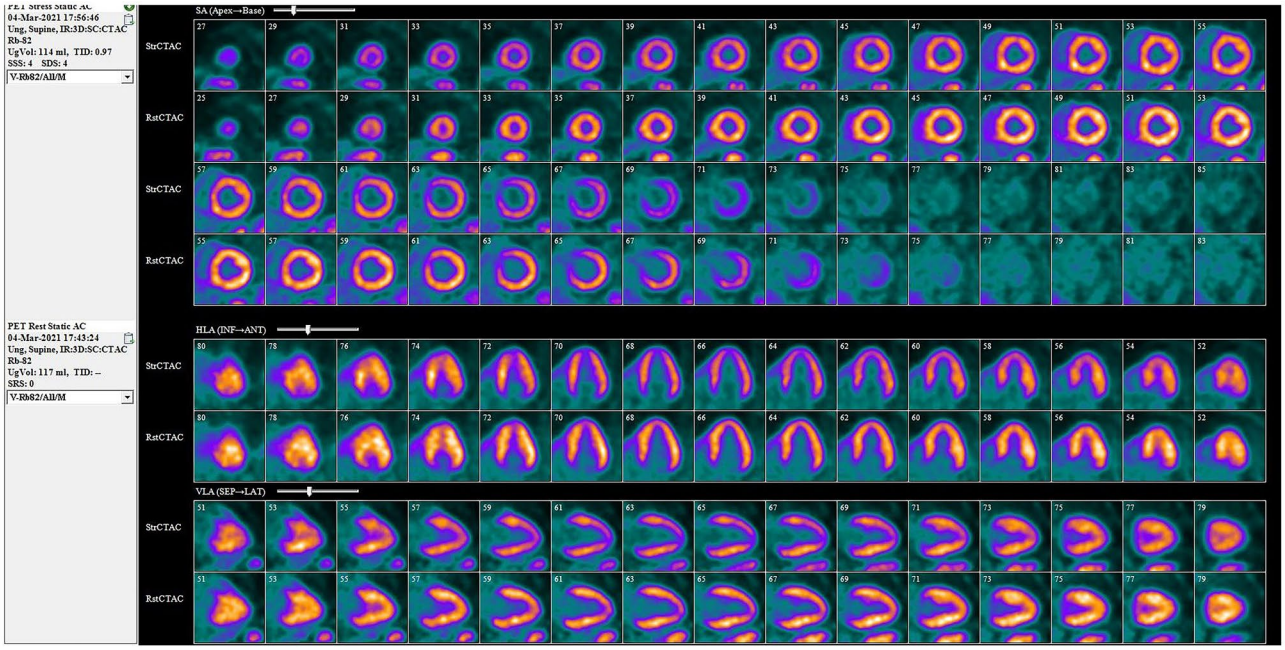

Fig. 5 ^{82}Rb stress PETCT perfusion images (**a**) in a 66-year-old diabetic with chest pain with extensive left main LAD and left circumflex coronary calcification. Minimal anteroapical reversible perfusion defect were present on PET (top panel). But global reduction in MFR was noted with flow analysis (**b**, bottom panel). Coronary angiography showed diffuse non-obstructive disease. Overall findings favored diffuse atherosclerosis plus concomitant microvascular dysfunction. Abbreviations: ^{82}Rb, Rubidium-82; LAD, left anterior descending; MFR, myocardial flow reserve; PET, positron emission tomography. Abbreviations: ANT, anterior; INF, inferior; LAD, left anterior descending artery; LAT, lateral; LCX, left circumflex artery; RCA, right coronary artery; ROI, region of interest; Rst, rest; SEP, septal; Str, stress

of 88% and 85%, and area under the curve of 0.95 and 0.90 for PET and SPECT, respectively [46]. Unlike SPECT, PET can also quantify MBF, which is a measure of microvascular function, and can help detect subclinical CAD as well as identify a balanced reduction in MBF in coronary arteries. In a study on 75 obese patients who underwent thallium-201 SPECT imaging, ^{82}Rb PET, and subsequent cardiac catheterization, PET was also found to have significantly greater specificity than SPECT (84% vs 64%) [47]. Bateman et al. reported that the overall diagnostic accuracy was much better for PET than SPECT at stenosis thresholds of 50% (87% vs 71%) and 70% (89% vs 79%) [48].

Cardiac PET has been found to be very useful not only for the diagnosis of CAD, but also for risk stratification in obese patients. In a study on 90 obese patients who were referred for PET after an equivocal SPECT, prognostic value of ^{82}Rb PET was evaluated. The annual rate of cardiac events was found to be only 1.3% in patients within normal PET MPI vs 15.2% in patients with abnormal PET MPI. In this study, in patients with normal ^{99m}Tc SPECT MPI, the vasodilator-induced changes in ECG were found to be associated with adverse outcomes even in the presence of a normal perfusion scan. However, patients with a normal ^{82}Rb PET MPI were found to have excellent prognosis, irrespective of vasodilator-induced ECG changes [49]. Another large multi-center study on 7061 patients by Chow et al. revealed that patients with normal PET MPI findings were found to have excellent prognosis in terms of annual rates of cardiac death [50].

Heart failure and myocardial viability

Normal myocardium has variable avidity for glucose and dietary carbohydrate intake triggers insulin secretion which activates glucose transporter GLUT4 in normal myocardium thereby allowing glucose to enter myocytes. In the absence of carbohydrates and insulin, the myocardium uses free fatty acids for energy. However, in inflammatory cells, glucose enters the cell via GLUT1 and GLUT3 which are constitutively expressed. After entering the myocyte via a glucose transporter, ^{18}F-FDGis trapped by phosphorylation, thereby allowing metabolic imaging. When using ^{18}F-FDG to assess myocardial viability, the substrate and hormonal level in the blood need to favor metabolism of glucose over fatty acids by the myocardium; therefore, a high insulin state is preferred. This increases the ^{18}F-FDG uptake in heart muscle, resulting in superior image quality and reducing regional uptake variations.

Standardized protocol involves loading the patient with glucose after a fasting period of at least 6 h to induce an endogenous insulin response. Increase in plasma glucose stimulates pancreatic insulin production, which in turn reduces plasma fatty acid levels and also normalizes plasma glucose levels. Glucose loading involves an oral load of 25 to 50 g but intravenous loading can also be used. Intravenous route avoids potential problems due to variable gastrointestinal absorption times or inability to tolerate oral loading.

FDG PET imaging is a well-accepted modality for hibernating myocardium assessment for myocardial metabolic integrity by glucose utilization concept [5, 6]. Although observational studies have clearly shown benefit of revascularizing hibernating myocardium, randomized trials have not shown survival benefit of revascularization as compared to optimal medical treatment [51–53]. Three randomized control trials, namely, the PET and recovery following revascularization (PARR-2) trial [51], the Heart Failure Revascularization (HEART) trial [52], and the surgical treatment for ischemic heart failure (STICH) trial [53] did not show clear survival benefit of revascularizing viable myocardium over medical treatment. However, these results are widely debated [54] as these trials had significant methodological limitations. European Society of Cardiology 2016 guidelines [55] recommended noninvasive stress imaging to assess for inducible ischemia and viable myocardium in patients with heart failure and CAD before the decision on revascularization [53]. Various studies have demonstrated a direct relationship between the number of dysfunctional viable segments and the magnitude of LVEF recovery after revascularization [56].

Chronic progressive CAD leads to reduction in blood flow as coronary obstruction worsens and resultant contractile dysfunction, which has potential to recover after revascularization (hibernating myocardium), and multiple modalities are available to evaluate hibernating myocardium [57–59].

To distinguish ischemic viable myocardium from the scar, FDG images are compared with perfusion images (^{13} N-NH_3 PET, ^{99m}Tc-Tetrofosmin, ^{99m}Tc-MIBI, and ^{201}Tl SPECT). Myocardial segments with reduced perfusion as well as reduced FDG uptake ("flow-metabolism match") suggest irreversible injury and nonviable myocardium (Table 3). On the other hand, segments with reduced perfusion but relatively preserved FDG uptake ("flow-metabolism mismatch") suggest viable myocardium as shown in Fig. 6.

Table 3 Various patterns of perfusion and metabolic uptake with ^{18}F-FDG

Perfusion	Metabolism	Interpretation
Normal	Normal	Viable myocardium
Reduced	Normal	Hibernating Myocardium
Reduced	Reduced	Non-viable myocardium
Normal	Reduced	Reverse mismatch (altered glucose metabolism)

The magnitude of flow-metabolism mismatch was found to have linear correlation with the magnitude of improvement in heart failure symptoms after revascularization. In elderly patients, viable myocardium detected by cardiac FDG PET/CT was found to be associated with better clinical outcomes when revascularized [59]. ^{18}F-FDG PET has a sensitivity and specificity of 92% and 63%, respectively, to predict improvement of regional function following revascularization.

PET imaging in heart failure provides data for diagnosis, prognosis, and disease monitoring [60]. PET and CMR scans are being used more frequently in the evaluation of heart failure patients, either simultaneously or separately, with application of post-acquisition fusion of independently acquired scans. Quantitative measurements of MBF and metabolism using PET provide state-of-the-art methodology for evaluation and management of patients at all stages of heart failure [61]. In early stages of heart failure, quantitative measurements of absolute MBF provide assessment of coronary microvascular function, which helps in prognostication [62] as well as in monitoring the response to therapy. In more advanced stages of heart failure, quantitative MBF and glucose metabolism by PET help in assessment of myocardial viability [52, 63], prognosis, and selection of patients for coronary revascularization [64]. Besides using PET to assess MBF and LVEF reserve, neurohormonal PET imaging is coming up as a promising tool to evaluate sympathetic innervation in heart failure [65, 66]. This is further discussed in detail in the "Emerging applications of PET" section.

In patients with heart failure with preserved ejection fraction and normal epicardial perfusion on cardiac PET, abnormal MFR is associated with LV diastolic dysfunction and reduced LV and LA strain.

Sarcoidosis

Sarcoidosis is a multisystem granulomatous disease that can cause inflammatory cardiomyopathy associated with arrhythmia, heart failure, and sudden cardiac death [67]. The diagnosis of cardiac involvement is challenging and often unrecognized. The Japanese Circulation Society Criteria (2017) and the Heart Rhythm Society criteria are used to establish diagnosis of cardiac sarcoidosis [68, 69]. FDG PET is a very well-established imaging modality for the diagnosis of extra-cardiac sarcoidosis, and it also plays a significant role in the diagnosis of cardiac sarcoidosis by detecting active inflammation in myocardium [8, 70]. In a meta-analysis of 17 studies with 891 patients, the pooled sensitivity, specificity, positive likelihood ratio, and negative likelihood ratio with ^{18} F-FDG PET/CT were found to be 84%, 83%, 4.9, and 0.2,

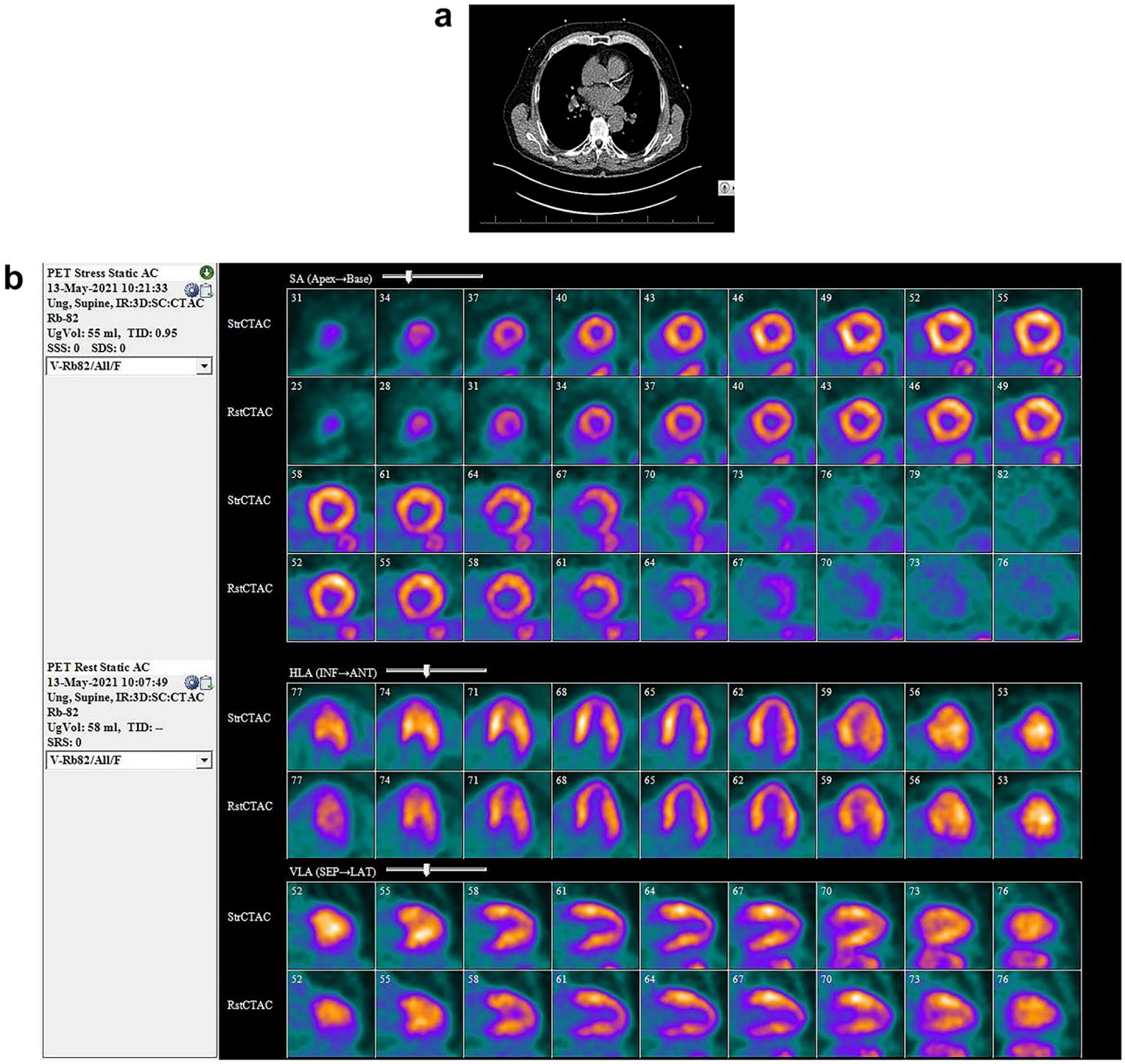

Fig. 6 Integrating coronary calcium information with ^{82}Rb stress PET and quantitative PET flow analysis. ^{82}Rb PET/CT in a 70-year-old man with abnormal electrocardiogram. Attenuation CT (**a**, top panel) shows extensive coronary calcification, but PET perfusion (**b**, bottom panel) was normal. Rest EF was 56% and stress EF was 62%. Thus atherosclerosis is identified warranting medical therapy to reduce long-term risk, yet short-term prognosis is good based on perfusion and hence no intervention is needed. Abbreviations: ^{82}Rb, Rubidium-82; ANT, anterior; CT, computed tomography; EF, ejection fraction; INF, inferior; LAT, lateral; PET, positron emission tomography; SEP, septal

respectively. Furthermore, the pooled diagnostic odds ratio was 27 (95% CI 14–55) with an area under the curve of 0.90. The moderate specificity and sensitivity of ^{18}F-FDG PET were further enhanced using combined MPI data [53] ^{18}F-FDG PET is also found to be helpful for monitoring therapy efficacy and for deciding treatment continuation or treatment change [8]. It is important to point out the FDG PET abnormalities in isolation cannot be used to diagnose sarcoidosis as focal FDG uptake is nonspecific and just denotes an area of inflammation.

FDG uptake on PET imaging is known as a surrogate for active inflammation [71], and late gadolinium enhancement on CMR is a surrogate for scar and fibrosis. PET provides information about myocardial and extra-cardiac

inflammation whereas CMR provides information about myocardial structure, function, and pattern of injury on late gadolinium enhancement [4]. Quantification parameters such as maximal and mean standardized uptake values, particularly at the basal septum, were found to be predictors of composite endpoint of ventricular tachycardia, automatic implantable cardioverter-defibrillator placement, complete heart block, pacemaker placement, atrial fibrillation, heart failure, and cardiac-related hospital admissions after a mean follow-up of 3 years [72].

An optimal FDG PET imaging for cardiac sarcoidosis necessitates adequate suppression of physiologic FDG uptake, which in turn is highly dependent on strict diet preparation prior to the study. Most centers are currently following low-no carbohydrate, high-fat diet, at least 10–12 h of fasting, and optional single bolus of intravenous heparin injection (which promotes lipolysis) to adequately suppress physiologic FDG uptake [73]. PET imaging for cardiac sarcoidosis includes simultaneous perfusion imaging as well as 18 F-FDG uptake imaging. Typical pattern for cardiac sarcoidosis includes mismatched perfusion-metabolic defects (Fig. 7). Other patterns include focal areas of uptake or less-specific focal on diffuse uptake of FDG (Fig. 8). Finally, perfusion defects with no myocardial uptake could suggest areas of scarring [74].

^{68}Ga-DOTA-conjugated peptides are newer radiotracers that have been found to be promising in diagnosing cardiac sarcoidosis because of their benefit of no physiologic uptake in myocardium [75].

Emerging applications of cardiac PET

Prosthetic valve endocarditis

Mechanical or biological prosthetic valve endocarditis (PVE) constitutes about 10–30% of all cases of infective endocarditis. Patients with prosthetic valves are at high risk of infective endocarditis, with an incidence of about 0.3–1.2% per patient-year [76, 77]. PVE is associated with high morbidity and mortality, with periannular complication rates above 50% and mortality rates reaching 30–50% [77]. Diagnosing PVE can be much more challenging as compared to native valve endocarditis, due to relatively atypical clinical presentation and lower sensitivity of Duke criteria for PVE [78]. The diagnosis of PVE is based on clinical

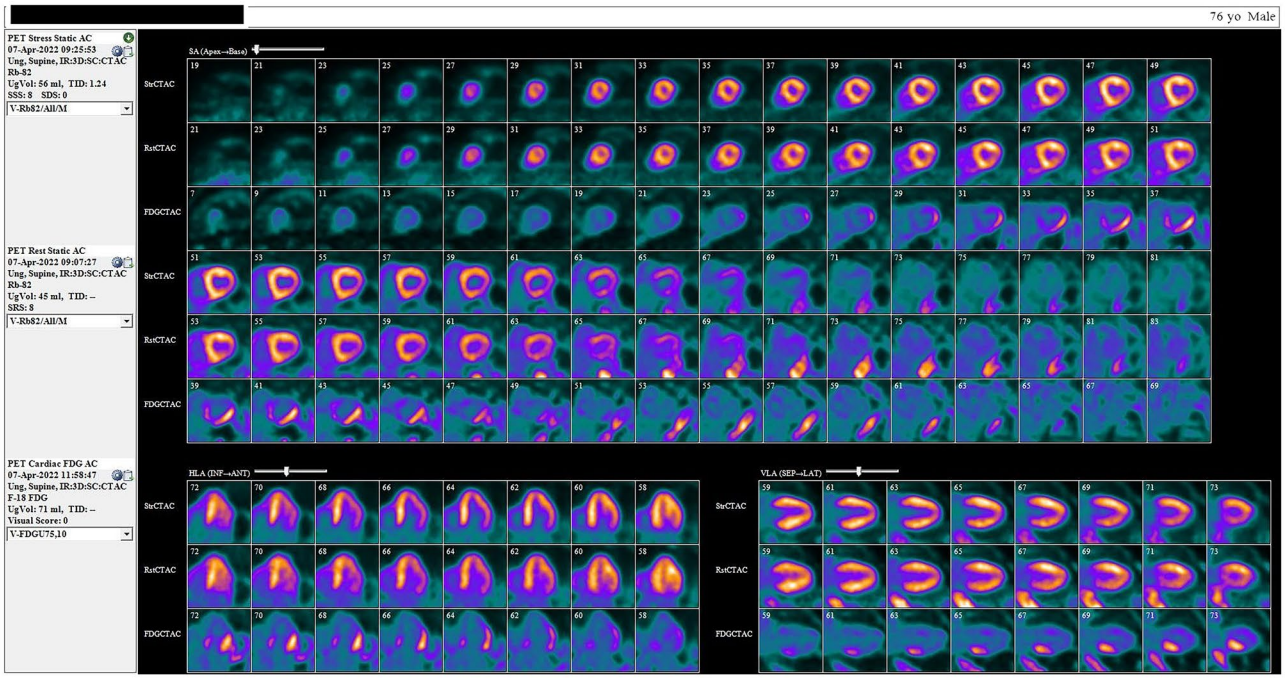

Fig. 7 A 62-year-old female with single vessel disease, known occluded dominant left circumflex artery, and prior fixed lateral wall defect suggesting infarct on SPECT presenting with angina like symptoms. PET rest-stress with FDG viability scan done for consideration of ischemia assessment and viability assessment for LCX CTO intervention. The rest-stress PET shows large predominantly fixed lateral wall defect, but FDG images show substantial hibernating myocardium with entire lateral wall uptake of FDG. She underwent successful recanalization of LCX CTO with significant symptom improvement. Abbreviations: ^{82}Rb, Rubidium-82; CTAC, computed tomography-based attenuation correction; CTO, chronic total occlusion; FDG, flourodeoxyglucose; LCX, left circumflex; PET, positron emission tomography

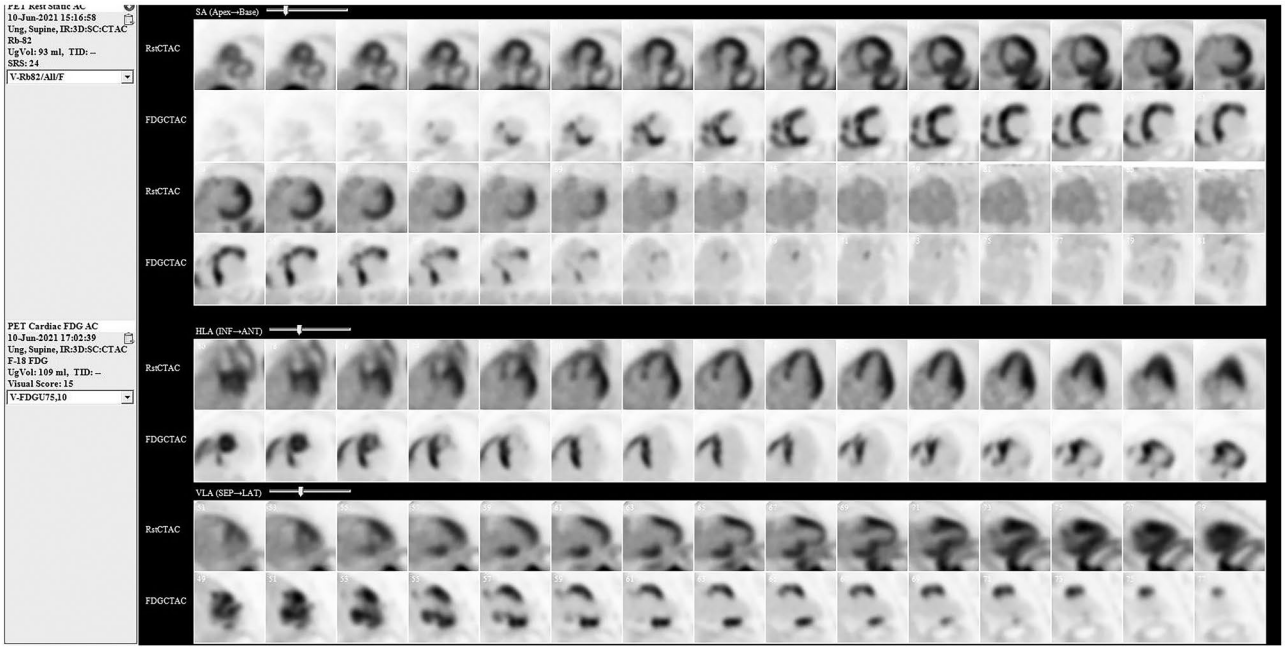

Fig. 8 A 60-year-old female with history of pulmonary sarcoidosis presenting with sudden syncopal episode. Twelve-lead electrocardiogram showed complete heart block. Cardiac catheterization showed no coronary artery disease, and she received a permanent pacemaker. ^{82}Rb ^{18}F-FDG PET was done to evaluate for cardiac sarcoidosis. Top images show large perfusion defect along the septum extending to basal anterior wall and perfusion defects in distal inferior wall. Metabolic images show substantial mismatch with FDG uptake in the septum parts of basal anterior wall and distal inferior wall. Patient was diagnosed with active cardiac sarcoidosis and initiated on steroids. Abbreviations: ^{82}Rb, Rubidium-82; ANT, anterior; CTAC, computed tomography–based attenuation correction; FDG, flourodeoxyglucose; HLA, horizontal long axis; INF, inferior; LAT, lateral; PET, positron emission tomography; Rst, rest; SA, short axis; SEP, septal; Str, stress; VLA, vertical long axis

signs and symptoms, blood cultures, and imaging. Transthoracic (TTE) and transesophageal echocardiograms (TEE) are still the mainstay of work-up; however, almost 30% of PVE patients show normal or inconclusive echocardiographic images [76, 78]. Cardiac CT has been used in the work-up, but it only offers anatomical information without providing functional data.

In recent years, nuclear imaging techniques, especially PET/CT with ^{18}F-FDG, have gained significant importance in work-up and diagnosis of PVE. Because of its ability to measure metabolic tissue activity, PET can locate metabolic or functional abnormalities and differentiate them from surrounding healthy tissues [77]. Meta-analyses and systematic reviews of several small studies [79, 80] evaluated the performance of FDG PET/CT for the diagnosis of PVE and reported a pooled sensitivity of 77% (95% CI 72–81%) and specificity of 78% (95% CI 72–83%) [79]. Furthermore, a prospective multicenter study on 115 patients reported sensitivity of 74%, specificity of 75%, positive predictive value of 91%, and negative predictive value of 42% [81]. In a recent study by de Camargo et al. on 188 patients with PVE/ascending aortic prosthesis infection, the sensitivity, specificity, and positive and negative predictive values of ^{18}F-FDG PET/CT focal uptake were 93%, 90%, 89%, and 94%, respectively [82].

FDG PET/CT provides incremental information to other imaging modalities, especially TTE and TEE. This, as a result, improved sensitivity of Duke criteria for diagnosis of PVE from 70 to 97% without reducing the specificity with addition of FDG PET/CT data. A significant proportion of patients with PVE can be reclassified from *Possible Infective Endocarditis* to *Definite Infective Endocarditis* category, resulting in a reduction of *Possible Infective Endocarditis* cases from 56 to 36%.

The 2015 European Society of Cardiology guidelines have recognized FDG PET/CT as a major criterion for the diagnosis of PVE [76]. Fig. 9 illustrates a case of PVE and the value of FDG PET in PVE. In recent years, novel radiotracers have been studied as alternatives to FDG to overcome the limitations of FDG seen early after prosthetic valve surgery as postoperative imaging can be associated with false positives or nonspecific uptake in inflamed tissue. Most studies have suggested waiting a minimum of 4–6 weeks after surgery to avoid such false positive findings [77].

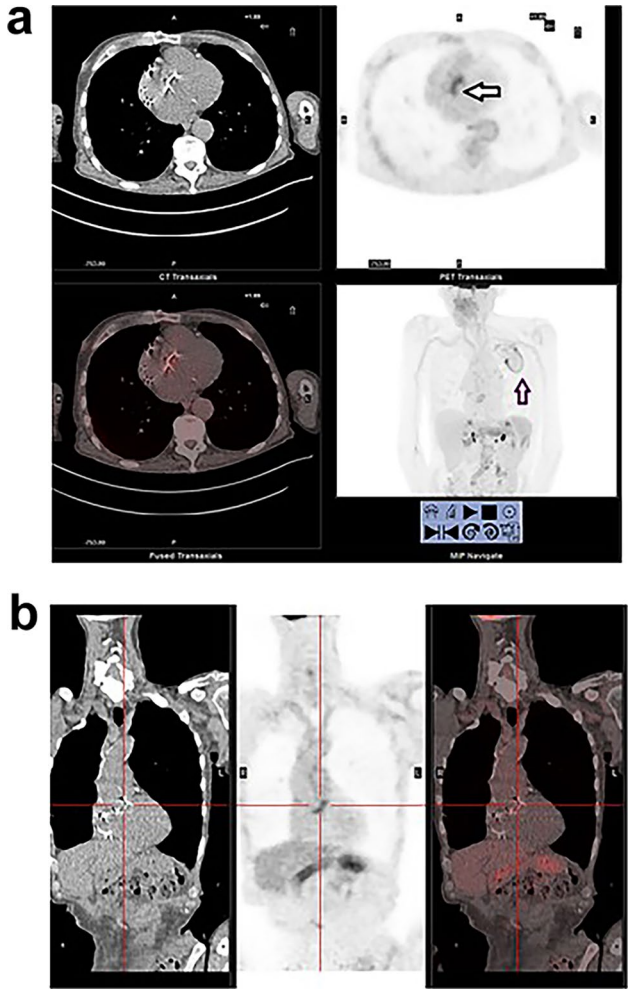

Fig. 9 An 84-year-old male with suspected prosthetic aortic valve endocarditis (valve replaced in 2006) with positive blood culture for *Streptococcus viridans*. Transthoracic echocardiogram showed probable vegetations. ^{18}F-FDG PET/CT shows uptake in the valve (horizontal arrow; SUVmax 3.5) suggesting infection. Uptake in the pacemaker pocket (vertical arrow) was considered reactive inflammatory changes related to recent implantation. Image courtesy of Dr. P. Arumugam and Dr. S. Muthu, Manchester University NHS Foundation Trust, Manchester, UK. Abbreviations: ^{82}Rb, Rubidium-82; CT, computed tomography; FDG, flourodeoxyglucose; PET, positron emission tomography; SUVmax, maximum standardized uptake value

Cardiac implantable electronic device infections

The presentation of cardiac implantable electronic device (CIED) infections can be quite variable in nature, extent, and severity. Moreover, they are often associated with involvement of extracardiac sites, which makes it more challenging to diagnose CIED infections [83]. These patients can present with superficial incisional infection, device pocket infection, systemic infection, or cardiac valve endocarditis. Diagnosis with high accuracy is important as management of respective conditions can differ considerably ranging from short course of antibiotics to debridement to complete CIED system explantation [84].

Echocardiography, TTE, and TEE are the mainstay of initial work-up for CIED infections. TTE is considered better in defining pericardial effusion, pulmonary vascular pressure, and ventricular dysfunction; TEE is considered superior in defining the presence and size of lead vegetations, particularly in the superior vena cava and right atrium [85]. However, both TTE and TEE may not be able to differentiate a sterile thrombus from infected vegetation. Furthermore, a negative echocardiogram does not exclude CIED lead endocarditis, due to its limited ability to visualize extracardiac portion of the CIED leads. Chest CT or ECG-gated CT angiogram may detect structural damage caused by the infection, such as abscesses or vegetations [83].

FDG PET/CT has emerged as a promising multimodality imaging technique capable of identifying infective foci and at an earlier stage, prior to development of morphological changes and extensive structural damage [83, 86]. PET/CT is now recommended in the diagnostic work-up and evaluation of suspected CIED infections [84] as the accuracy of PET/CT has been found to be very good, especially for diagnosis of CIED generator pocket infections [87, 88]. The inflammatory changes secondary to device implantation usually resolve within about 6 weeks of the procedure. Any FDG uptake beyond this time period is usually concerning for an infectious process.

Figure 10 is an example of PET/CT found to be very useful in differentiating true pocket infection from superficial incisional infection, thereby helping in deciding on an optimal management plan [89]. In a meta-analysis of 14 studies for diagnosis of local pocket infections, PET/CT was found to have pooled sensitivity of 96% and pooled specificity of 97%; and for diagnosis of CIED lead infections, the pooled sensitivity was 76% and specificity was 83% [90]. The ability to scan the whole body with FDG PET/CT is quite useful in detecting embolic foci and metastatic sites of infection, such as pulmonary emboli, splenic emboli, spine infections, and mycotic aneurysms. These extracardiac findings can further support the diagnosis of lead or valvular endocarditis as well as help guide appropriate antimicrobial regimen and decision to explant the device.

PET/CT may provide prognostic information as shown by Diemberger et al.; they reported significantly increased mortality in patients with PET/CT evidence of lead infection, without pocket involvement. These patients were more likely to have *Staphylococcus aureus* infection, positive blood cultures, and vegetations, all of which were concerning for a non-pocket-related source of endovascular infection [91].

PET/CT also has high diagnostic accuracy for left ventricular assist device infections, with sensitivity of 87–100% and specificity of 79–91% [92]. In a study by de Vaugelade et al. where patients underwent both PET/CT and white

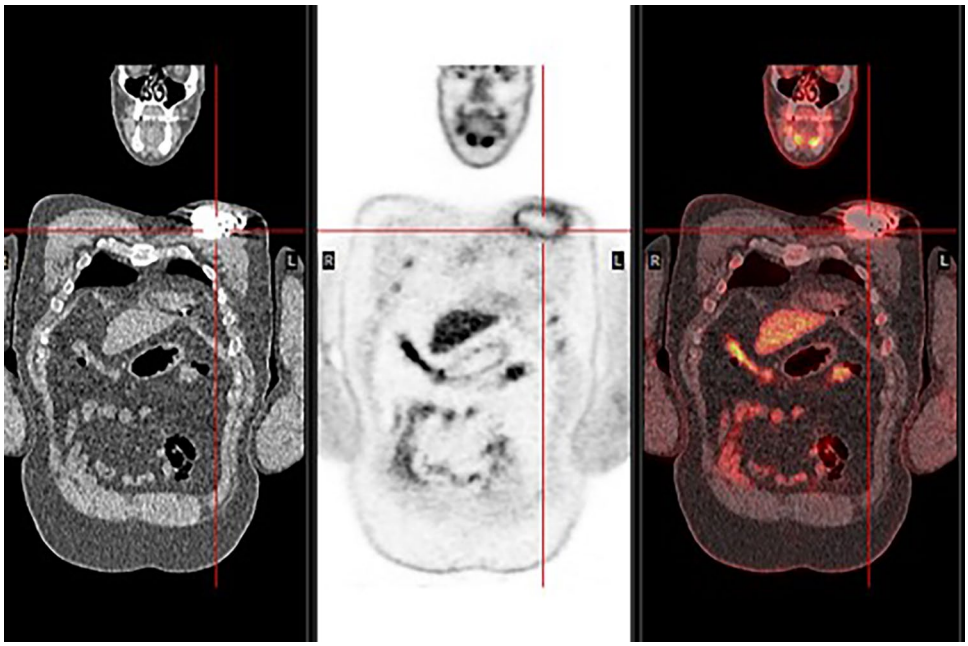

Fig. 10 A 69-year-old male with ICD for primary prevention in 2020. Local tenderness and redness at site of pocket. ^{18}F-FDG PET/CT shows circumferential heterogeneous increased uptake around the generator box, prominent uptake is seen superiorly with SUVmax 5.3 with no extension to the ICD leads. Image courtesy: Dr. P. Arumugam and Dr. S. Muthu, Manchester University NHS Foundation Trust, Machester, UK. Abbreviations: ^{18}F-FDG PET/CT, flourine-18 flourodeoxyglucose positron emission tomography computed tomography; ICD, implantable cardioverter defibrillator; SUVmax, maximum standardized uptake value

blood cell SPECT, the sensitivity and specificity of PET/CT were 95.2% and 66.7%, respectively, compared to 71.4% and 100% for white blood cell SPECT [93]. Given the higher specificity of white blood cell SPECT, it may be appropriate to perform this if suspicion of left ventricular assist device infection is high or PET/CT results are equivocal. Finally, PET/CT imaging has also been found useful in serial monitoring of cardiovascular infections to assess the response to antibiotic therapy.

Hypertrophic cardiomyopathy

Hypertrophic cardiomyopathy (HCM) is characterized by asymmetric left ventricular hypertrophy in the absence of any other cardiac or systemic disease. Symptoms and clinical course of HCM can vary significantly, ranging from the patient being totally asymptomatic to a wide range of complications including refractory heart failure, repetitive syncope, angina, or sudden cardiac death. Literature indicates that a significant proportion of HCM patients have stress-induced perfusion defects as well as functional abnormalities, secondary to the following 4 mechanisms: (1) increased energy demand of hypertrophic myocardium, (2) inflammatory response caused by inflammatory cells, (3) demand myocardial ischemia due to supply/demand mismatch, and (4) myocardial ischemia due to microangiopathy and coronary microvascular dysfunction [94]. Quantitative myocardial perfusion PET has emerged as an effective tool for measuring MBF and assessing coronary microvascular dysfunction. PET can quantify MBF to identify these subendocardial perfusion abnormalities in HCM patients. Figure 11 is a case example of a patient with mid-apical hypertrophic obstructive cardiomyopathy and chest pain. Significant ischemia was seen in the left anterior descending distribution, but coronary angiography showed no obstructive CAD, thus confirming the etiology of ischemic response was likely microvascular dysfunction. Also of note, the resting perfusion images showed increased radioisotope uptake in mid apical segments related to asymmetric hypertrophy.

Aoyama et al. in their study on HCM patients also found that ^{18}F-FDG uptake was increased in hypertrophied myocardium in hypertrophic nonobstructive cardiomyopathy patients, whereas uptake was extensively accumulated beyond the hypertrophied myocardium in hypertrophic obstructive cardiomyopathy patients. Also, the extent of FDG uptake was closely related to troponin level, as well as degree of LV diastolic dysfunction and brain natriuretic peptide levels [95].

Aortic stenosis

Cardiac PET when used with CT/MR provides benefits of both anatomical and molecular techniques for comprehensive imaging assessment of aortic stenosis (AS). PET/CT can be used to measure inflammation and valvular calcification activity in AS, thereby providing important insights into the pathogenesis as well as serving as a useful surrogate endpoint of disease activity [96].

Angina is one of the common symptoms in AS patients, but interestingly about one-fourth of these patients have no significant epicardial CAD. Angina in these patients is attributed to decreased MFR with chronic pressure overload.

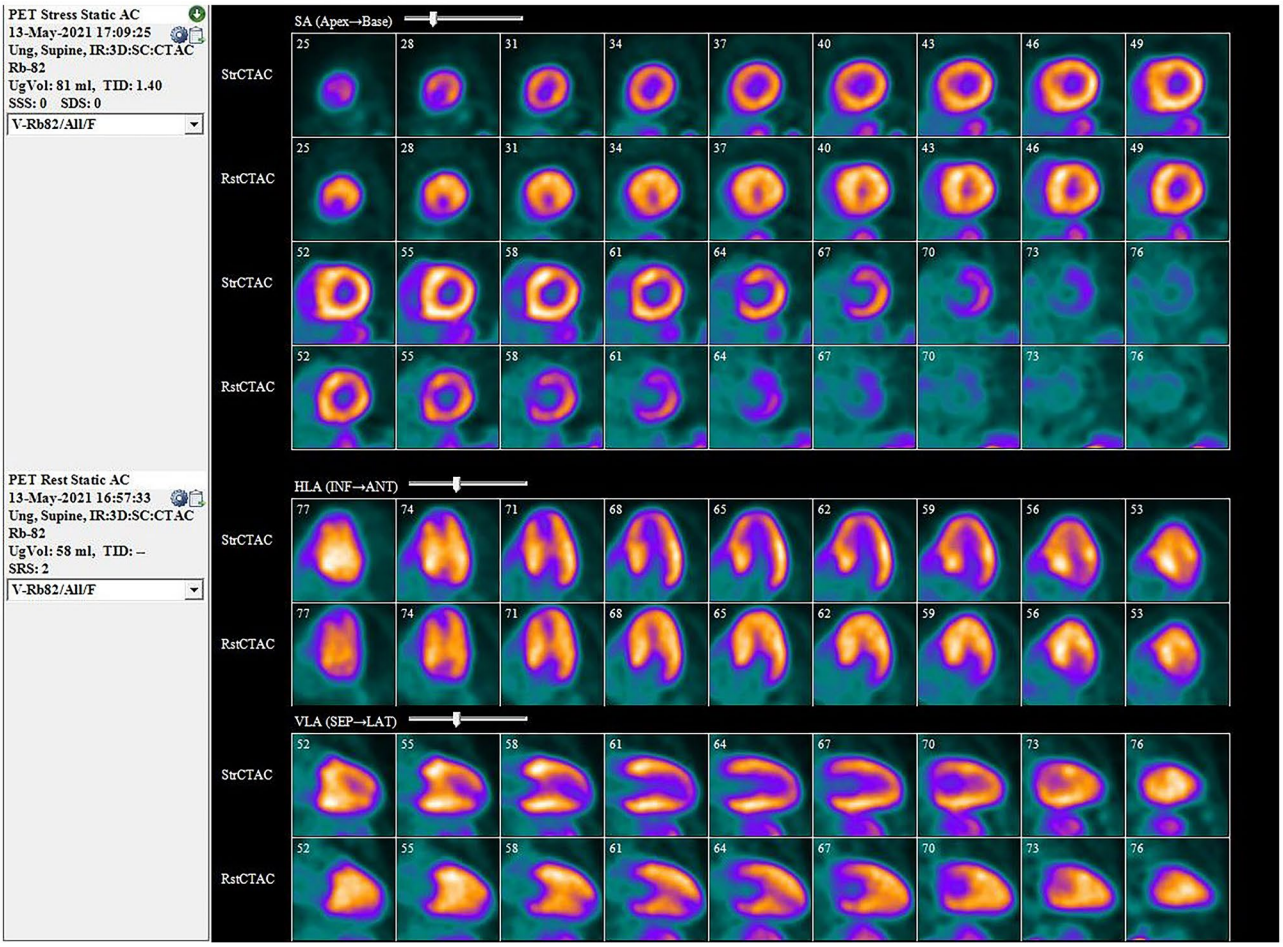

Fig. 11 A 70-year-old female with apical hypertrophic cardiomyopathy with chest pain. ^{82}Rb rest-stress regadenoson PET shows moderate sized, moderate intensity reversible perfusion defect in the mid-distal anterior wall, septum, and apex and peri-apical areas. The rest image shows asymmetric intense uptake of isotope in the mid-distal ventricular myocardium corresponding to asymmetric apical hypertrophic cardiomyopathy phenotype. Coronary angiography showed nonobstructive disease confirming that the observed ischemic defect was related to other mechanisms including microvascular dysfunction. Abbreviations: ^{82}Rb, Rubidium-82; AC, attenuation correction; Ant, anterior; Horiz, horizontal; Lat, lateral; PET, positron emission tomography; Post, posterior; Rst, rest; Sep, septal; Str, stress; Vert, vertical

Pathophysiology for decreased MFR in AS has 3 proposed mechanisms: capillary rarefaction, perivascular fibrosis, and reversal of endo-epicardial gradient [97]. Impairment of MFR is thought to cause subendocardial ischemia and, subsequently, myocardial apoptosis. Zhou et al. in a recent study hypothesized that subendocardial ischemia in AS leads to progressive abnormalities in MFR and, ultimately, subclinical LV dysfunction [98]. This study further suggested emerging role of cardiac PET and MBF assessment to identify the high-risk subset of AS patients as patients with abnormal MFR had worse outcomes when compared to patients with normal MFR over the 7.2 median years of follow-up. In an expert review regarding the role of multimodality imaging in AS, the Heart Valve Clinic International Database Group has proposed a potential role of advanced imaging, including PET, to further risk stratify challenging subsets of AS patients [99].

Cardiac autonomic neuronal function

The primary extrinsic control of cardiac performance in human body comes from autonomic nervous system. Altered autonomic activity plays an important role in the progression of various cardiac pathologies. Some studies have shown a mechanistic role for heterogeneous sympathetic innervation causing life-threatening ventricular arrhythmias [48]. ^{123}I-Metaiodobenzylguanidine (^{123}I-MIBG) is commonly used radiotracer for SPECT and ^{11}C-metahydroxephedrine (^{11}C-HED) is the most commonly used radiolabeled catecholamine tracer for PET imaging in humans. Uptake of these

radiotracers is a reflection of neuronal integrity. The extent of decrease in ^{11}C-HED uptake in heart failure patients correlated well with their New York Heart Association functional classification and EF. This decrease in the extent of ^{11}C-HED uptake was also found to be an independent predictor for sudden cardiac death in ischemic cardiomyopathy as well as for combined endpoint of death or cardiac transplantation [49].

^{123}I-MIBG predominantly emits 159-keV gamma rays but also admits low-abundance high-energy 529-keV rays which can affect image quality. ^{123}I-MIBG also accumulates in the liver and lungs thereby affecting image quality. Imaging in prone position has been shown to improve image quality thereby improving prognostic value of SPECT myocardial perfusion imaging. On the other hand, ^{11}CHED has homogeneous tracer distribution thereby providing much better resolution which allows improved regional analysis and kinetic modeling, thereby providing much better quantification. However, the requirement of onsite cyclotron and specialized centers for interpretation and radiosynthesis limits overall clinical application.

Limitations of PET

Although the advantages and myriad applications of cardiac PET have been well outlined, PET/CT imaging can be associated with several limitations, some unique to the technology and some similar to SPECT [8]. These include inadequate patient preparation, motion scatter, and PET/CT mismatch artifacts. Issues related to inadequate patient preparation for viability studies include elevated blood glucose leading to no suppression of myocardial uptake, and use of interfering drugs such as antibiotics and steroids resulting in reduced sensitivity of ^{18}F-FDG PET/CT. For stress PET, inadequate preparation includes caffeine consumption which can decrease sensitivity of vasodilator stress. Issues leading to acquisition artifacts include motion, metal/scatter/beam–hardening/calcification artifacts, arrhythmias, and suboptimal standardization. Furthermore there are reconstruction related artifacts such as truncation and mismatch of fusion of PET and CT. Finally, issues related to reading errors are usually secondary to false positive uptake in surrounding tissue, various pathological conditions such thrombi or tumor, and a short interval between surgery and imaging.

PET/MR hybrid imaging also comes with certain limitations. The primary technical challenge is attenuation correction, which is the process through which the collected data are corrected for attenuation caused by body tissues and the components of the MR scanner. As compared to PET/MR, PET/CT provides more accurate attenuation correction because the Hounsfield unit of x-ray attenuation is more accurately transformed into equivalent linear attenuation coefficient for PET photons [4]. Another limitation is attenuation correction at the edge of the field of view as the magnetic field becomes inhomogeneous in that area, especially in the obese population. Metallic implants, including coronary stents and prosthetic valves, also lead to artifacts that are more pronounced in MR imaging as compared to CT imaging. Another limitation of PET/MR scans is that they are much more expensive as compared to other imaging modalities both in their initial cost as well as running cost.

Conclusions

Cardiac PET and hybrid PET imaging with PET/CT and PET/MR imaging have proved themselves as precise imaging modalities that provide functional imaging of the heart in addition to anatomical imaging. Cardiac PET has established itself as one of the best available techniques for evaluation of myocardial viability. It is also recommended for the optimal management of reduced LV function and ischemic cardiomyopathy. Hybrid PET/CT provides simultaneous integration of coronary anatomy and function with myocardial perfusion and metabolism, thereby improving characterization of the dysfunctional area and chronic CAD. The availability of quantitative MBF evaluation with PET provides additional prognostic information and increases diagnostic accuracy in management of patients with CAD. Hybrid imaging seems to hold immense potential in optimizing management of cardiovascular diseases and furthering clinical research.

Future cardiac PET research lies in further understanding and development of molecular imaging and in establishing new perfusion tracers that are more specific for particular etiologies, like sarcoidosis and amyloidosis. Another area of research lies in the development of perfusion tracers suitable for PET imaging at centers without an on-site cyclotron facility.

Author contribution Amit Bansal, Karthikeyan Ananthasubramaniam: conceptualization; methodology; data curation; writing—original draft preparation; visualization; investigation. Karthikeyan Ananthasubramaniam: supervision; Amit Bansal, Karthikeyan Ananthasubramaniam, Stephanie Stebens: writing—reviewing and editing.

Availability of data and materials Not applicable.

Declarations

Ethical approval Not applicable.

Competing interests Not applicable.

References

1. Ter-Pogossian MM, Phelps ME, Hoffman EJ, Mullani NA (1975) A positron-emission transaxial tomograph for nuclear imaging (PETT). Radiology 114:89–98

2. Gaemperli O, Kaufmann PA (2011) PET and PET/CT in cardiovascular disease. Ann N Y Acad Sci 1228:109–136
3. Townsend DW (2008) Positron emission tomography/computed tomography. Semin Nucl Med 38:152–166
4. Robson PM, Dey D, Newby DE et al (2017) MR/PET imaging of the cardiovascular system. JACC Cardiovasc Imaging 10:1165–1179
5. Klein C, Nekolla SG, Bengel FM et al (2002) Assessment of myocardial viability with contrast-enhanced magnetic resonance imaging: comparison with positron emission tomography. Circulation 105:162–167
6. Schwitter J, DeMarco T, Kneifel S et al (2000) Magnetic resonance-based assessment of global coronary flow and flow reserve and its relation to left ventricular functional parameters: a comparison with positron emission tomography. Circulation 101:2696–2702
7. Boyd DP (2007) Instrumentation and principles of CT. In: Di Carli MF, Lipton MJ (eds) Cardiac PET and PET/CT Imaging. Springer, New York, pp 19–33
8. Slart R, Glaudemans A, Gheysens O et al (2021) Procedural recommendations of cardiac PET/CT imaging: standardization in inflammatory-, infective-, infiltrative-, and innervation (4Is)-related cardiovascular diseases: a joint collaboration of the EACVI and the EANM. Eur J Nucl Med Mol Imaging 48:1016–1039
9. Araujo LI, Lammertsma AA, Rhodes CG et al (1991) Noninvasive quantification of regional myocardial blood flow in coronary artery disease with oxygen-15-labeled carbon dioxide inhalation and positron emission tomography. Circulation 83:875–885
10. Schelbert HR, Phelps ME, Hoffman EJ, Huang SC, Selin CE, Kuhl DE (1979) Regional myocardial perfusion assessed with N-13 labeled ammonia and positron emission computerized axial tomography. Am J Cardiol 43:209–218
11. Herrero P, Markham J, Shelton ME, Weinheimer CJ, Bergmann SR (1990) Noninvasive quantification of regional myocardial perfusion with rubidium-82 and positron emission tomography. Exploration of a mathematical model Circulation 82:1377–1386
12. Nekolla SG, Reder S, Saraste A et al (2009) Evaluation of the novel myocardial perfusion positron-emission tomography tracer 18F-BMS-747158-02: comparison to 13N-ammonia and validation with microspheres in a pig model. Circulation 119:2333–2342
13. Maddahi J, Czernin J, Lazewatsky J et al (2011) Phase I, first-in-human study of BMS747158, a novel 18F-labeled tracer for myocardial perfusion PET: dosimetry, biodistribution, safety, and imaging characteristics after a single injection at rest. J Nucl Med 52:1490–1498
14. Veltman CE, de Wit-van der Veen BJ, de Roos A, Schuijf JD et al (2013) Myocardial perfusion imaging: the role of SPECT, PET and CMR. In: Marzullo P, Mariani G, eds. From Basic Cardiac Imaging to Image Fusion: Core Competencies Versus Technological Progress. Milan: Springer; 2013:29–49.
15. Yoshida K, Mullani N, Gould KL (1996) Coronary flow and flow reserve by PET simplified for clinical applications using rubidium-82 or nitrogen-13-ammonia. J Nucl Med 37:1701–1712
16. Lecomte R (2004) Technology challenges in small animal PET imaging. Nucl Instrum Methods Phys Res A 527:157–165
17. Yoshinaga K, Klein R, Tamaki N (2010) Generator-produced rubidium-82 positron emission tomography myocardial perfusion imaging-From basic aspects to clinical applications. J Cardiol 55:163–173
18. Yu M, Guaraldi MT, Mistry M et al (2007) BMS-747158-02: a novel PET myocardial perfusion imaging agent. J Nucl Cardiol 14:789–798
19. Krivokapich J, Huang SC, Selin CE, Phelps ME (1987) Fluorodeoxyglucose rate constants, lumped constant, and glucose metabolic rate in rabbit heart. Am J Physiol 252:H777-787
20. Kazakauskaite E, Zaliaduonyte-Peksiene D, Rumbinaite E, Kersulis J, Kulakiene I, Jurkevicius R (2018) Positron emission tomography in the diagnosis and management of coronary artery disease. Medicina (Kaunas) 54:47
21. Al Badarin FJ, Malhotra S (2019) Diagnosis and prognosis of coronary artery disease with SPECT and PET. Curr Cardiol Rep 21:57
22. Schindler TH, Zhang XL, Vincenti G, Mhiri L, Lerch R, Schelbert HR (2007) Role of PET in the evaluation and understanding of coronary physiology. J Nucl Cardiol 14:589–603
23. Camici PG, Crea F (2007) Coronary microvascular dysfunction. N Engl J Med 356:830–840
24. Schindler TH, Facta AD, Prior JO et al (2009) Structural alterations of the coronary arterial wall are associated with myocardial flow heterogeneity in type 2 diabetes mellitus. Eur J Nucl Med Mol Imaging 36:219–229
25. Shaw LJ, Min JK, Hachamovitch R et al (2010) Cardiovascular imaging research at the crossroads. JACC Cardiovasc Imaging 3:316–324
26. Dorbala S, Vangala D, Sampson U, Limaye A, Kwong R, Di Carli MF (2007) Value of vasodilator left ventricular ejection fraction reserve in evaluating the magnitude of myocardium at risk and the extent of angiographic coronary artery disease: a 82Rb PET/CT study. J Nucl Med 48:349–358
27. Lertsburapa K, Ahlberg AW, Bateman TM et al (2008) Independent and incremental prognostic value of left ventricular ejection fraction determined by stress gated rubidium 82 PET imaging in patients with known or suspected coronary artery disease. J Nucl Cardiol 15:745–753
28. Berman DS, Kang X, Slomka PJ et al (2007) Underestimation of extent of ischemia by gated SPECT myocardial perfusion imaging in patients with left main coronary artery disease. J Nucl Cardiol 14:521–528
29. Gould KL (2009) Coronary flow reserve and pharmacologic stress perfusion imaging: beginnings and evolution. JACC Cardiovasc Imaging 2:664–669
30. Tio RA, Dabeshlim A, Siebelink HM et al (2009) Comparison between the prognostic value of left ventricular function and myocardial perfusion reserve in patients with ischemic heart disease. J Nucl Med 50:214–219
31. Dayanikli F, Grambow D, Muzik O, Mosca L, Rubenfire M, Schwaiger M (1994) Early detection of abnormal coronary flow reserve in asymptomatic men at high risk for coronary artery disease using positron emission tomography. Circulation 90:808–817
32. Adenaw N, Salerno M (2013) PET/MRI: current state of the art and future potential for cardiovascular applications. J Nucl Cardiol 20:976–989
33. Valenta I, Quercioli A, Schindler TH (2014) Diagnostic value of PET-measured longitudinal flow gradient for the identification of coronary artery disease. JACC Cardiovasc Imaging 7:387–396
34. Schneider JF, Thomas HE Jr, Sorlie P, Kreger BE, McNamara PM, Kannel WB (1981) Comparative features of newly acquired left and right bundle branch block in the general population: the Framingham study. Am J Cardiol 47:931–940
35. Vernooy K, Verbeek XA, Peschar M et al (2005) Left bundle branch block induces ventricular remodelling and functional septal hypoperfusion. Eur Heart J 26:91–98
36. Hayat SA, Dwivedi G, Jacobsen A, Lim TK, Kinsey C, Senior R (2008) Effects of left bundle-branch block on cardiac structure, function, perfusion, and perfusion reserve: implications for myocardial contrast echocardiography versus radionuclide perfusion imaging for the detection of coronary artery disease. Circulation 117:1832–1841
37. Hoefflinghaus T, Husmann L, Valenta I et al (2008) Role of attenuation correction to discriminate defects caused by left bundle branch block versus coronary stenosis in single photon emission computed tomography myocardial perfusion imaging. Clin Nucl Med 33:748–751

38. Vaduganathan P, He ZX, Raghavan C, Mahmarian JJ, Verani MS (1996) Detection of left anterior descending coronary artery stenosis in patients with left bundle branch block: exercise, adenosine or dobutamine imaging? J Am Coll Cardiol 28:543–550
39. Falcao A, Chalela W, Giorgi MC et al (2015) Myocardial blood flow assessment with 82rubidium-PET imaging in patients with left bundle branch block. Clinics (Sao Paulo) 70:726–732
40. Ghotbi AA, Kjaer A, Hasbak P (2014) Review: comparison of PET rubidium-82 with conventional SPECT myocardial perfusion imaging. Clin Physiol Funct Imaging 34:163–170
41. Cremer P, Brunken R, Menon V, Cerqueira M, Jaber W (2015) Septal perfusion abnormalities are common in regadenoson spect myocardial perfusion imaging (MPI) but Not PET MPI in patients with left bundle branch block (LBBB) [abstract]. J Am Coll Cardiol 65:A1148
42. Vidula MK, Wiener P, Selvaraj S et al (2021) Diagnostic accuracy of SPECT and PET myocardial perfusion imaging in patients with left bundle branch block or ventricular-paced rhythm. J Nucl Cardiol 28:981–988
43. Arasaratnam P, Ayoub C, Klein R, DeKemp R, Beanlands RS, Chow BJW (2014) Positron emission tomography myocardial perfusion imaging for diagnosis and risk stratification in obese patients. Curr Cardiovasc Imaging Rep 8:9304
44. Machac J (2005) Cardiac positron emission tomography imaging. Semin Nucl Med 35:17–36
45. Ghanem MA, Kazim NA, Elgazzar AH (2011) Impact of obesity on nuclear medicine imaging. J Nucl Med Technol 39:40–50
46. Mc Ardle BA, Dowsley TF, deKemp RA, Wells GA, Beanlands RS (2012) Does rubidium-82 PET have superior accuracy to SPECT perfusion imaging for the diagnosis of obstructive coronary disease?: A systematic review and meta-analysis. J Am Coll Cardiol 60:1828–1837
47. Freedman N, Schechter D, Klein M, Marciano R, Rozenman Y, Chisin R (2000) SPECT attenuation artifacts in normal and overweight persons: insights from a retrospective comparison of Rb-82 positron emission tomography and TI-201 SPECT myocardial perfusion imaging. Clin Nucl Med 25:1019–1023
48. Bateman TM, Heller GV, McGhie AI et al (2006) Diagnostic accuracy of rest/stress ECG-gated Rb-82 myocardial perfusion PET: comparison with ECG-gated Tc-99m sestamibi SPECT. J Nucl Cardiol 13:24–33
49. Klodas E, Miller TD, Christian TF, Hodge DO, Gibbons RJ (2003) Prognostic significance of ischemic electrocardiographic changes during vasodilator stress testing in patients with normal SPECT images. J Nucl Cardiol 10:4–8
50. Chow BJ, Dorbala S, Di Carli MF et al (2014) Prognostic value of PET myocardial perfusion imaging in obese patients. JACC Cardiovasc Imaging 7:278–287
51. Beanlands RS, Nichol G, Huszti E et al (2007) F-18-fluorodeoxyglucose positron emission tomography imaging-assisted management of patients with severe left ventricular dysfunction and suspected coronary disease: a randomized, controlled trial (PARR-2). J Am Coll Cardiol 50:2002–2012
52. Cleland JG, Calvert M, Freemantle N et al (2011) The Heart Failure Revascularisation Trial (HEART). Eur J Heart Fail 13:227–233
53. Bonow RO, Maurer G, Lee KL et al (2011) Myocardial viability and survival in ischemic left ventricular dysfunction. N Engl J Med 364:1617–1625
54. Shah BN, Khattar RS, Senior R (2013) The hibernating myocardium: current concepts, diagnostic dilemmas, and clinical challenges in the post-STICH era. Eur Heart J 34:1323–1336
55. Ponikowski P, Voors AA, Anker SD et al (2016) 2016 ESC guidelines for the diagnosis and treatment of acute and chronic heart failure. Rev Esp Cardiol (Engl Ed) 69:1167
56. Ling LF, Marwick TH, Flores DR et al (2013) Identification of therapeutic benefit from revascularization in patients with left ventricular systolic dysfunction: inducible ischemia versus hibernating myocardium. Circ Cardiovasc Imaging 6:363–372
57. Barnes E, Dutka DP, Khan M, Camici PG, Hall RJ (2002) Effect of repeated episodes of reversible myocardial ischemia on myocardial blood flow and function in humans. Am J Physiol Heart Circ Physiol 282:H1603-1608
58. Wijns W, Vatner SF, Camici PG (1998) Hibernating myocardium. N Engl J Med 339:173–181
59. Namdar M, Rager O, Priamo J et al (2018) Prognostic value of revascularising viable myocardium in elderly patients with stable coronary artery disease and left ventricular dysfunction: a PET/CT study. Int J Cardiovasc Imaging 34:1673–1678
60. Quail MA, Sinusas AJ (2017) PET-CMR in heart failure - synergistic or redundant imaging? Heart Fail Rev 22:477–489
61. Gewirtz H (2011) Cardiac PET: a versatile, quantitative measurement tool for heart failure management. JACC Cardiovasc Imaging 4:292–302
62. Cecchi F, Olivotto I, Gistri R, Lorenzoni R, Chiriatti G, Camici PG (2003) Coronary microvascular dysfunction and prognosis in hypertrophic cardiomyopathy. N Engl J Med 349:1027–1035
63. Beanlands RS, deKemp R, Scheffel A et al (1997) Can nitrogen-13 ammonia kinetic modeling define myocardial viability independent of fluorine-18 fluorodeoxyglucose? J Am Coll Cardiol 29:537–543
64. Abraham A, Nichol G, Williams KA et al (2010) 18F-FDG PET imaging of myocardial viability in an experienced center with access to 18F-FDG and integration with clinical management teams: the Ottawa-FIVE substudy of the PARR 2 trial. J Nucl Med 51:567–574
65. Thackeray JT, Bengel FM (2013) Assessment of cardiac autonomic neuronal function using PET imaging. J Nucl Cardiol 20:150–165
66. Fallavollita JA, Heavey BM, Luisi AJ Jr et al (2014) Regional myocardial sympathetic denervation predicts the risk of sudden cardiac arrest in ischemic cardiomyopathy. J Am Coll Cardiol 63:141–149
67. Schatka I, Bengel FM (2014) Advanced imaging of cardiac sarcoidosis. J Nucl Med 55:99–106
68. Terasaki F, Azuma A, Anzai T et al (2019) JCS 2016 guideline on diagnosis and treatment of cardiac sarcoidosis - digest version. Circ J 83:2329–2388
69. Birnie DH, Sauer WH, Bogun F et al (2014) HRS expert consensus statement on the diagnosis and management of arrhythmias associated with cardiac sarcoidosis. Heart Rhythm 11:1305–1323
70. Kim SJ, Pak K, Kim K (2020) Diagnostic performance of F-18 FDG PET for detection of cardiac sarcoidosis; a systematic review and meta-analysis. J Nucl Cardiol 27:2103–2115
71. Sperry BW, Tamarappoo BK, Oldan JD et al (2018) Prognostic impact of extent, severity, and heterogeneity of abnormalities on ^{18}F-FDG PET scans for suspected cardiac sarcoidosis. JACC Cardiovasc Imaging 11:336–345
72. Flores RJ, Flaherty KR, Jin Z, Bokhari S (2020) The prognostic value of quantitating and localizing F-18 FDG uptake in cardiac sarcoidosis. J Nucl Cardiol 27:2003–2010
73. Schwartz RG, Malhotra S (2020) Optimizing cardiac sarcoid imaging with FDG PET: lessons from studies of physiologic regulation of myocardial fuel substrate utilization. J Nucl Cardiol 27:490–493
74. Slart R, Glaudemans A, Lancellotti P et al (2018) A joint procedural position statement on imaging in cardiac sarcoidosis: from the Cardiovascular and Inflammation & Infection Committees of the European Association of Nuclear Medicine, the European Association of Cardiovascular Imaging, and the American Society of Nuclear Cardiology. J Nucl Cardiol 25:298–319
75. Gormsen LC, Haraldsen A, Kramer S, Dias AH, Kim WY, Borghammer P (2016) A dual tracer ^{68}Ga-DOTANOC PET/CT and ^{18}F-FDG PET/CT pilot study for detection of cardiac sarcoidosis. EJNMMI Res 6:52

76. Habib G, Lancellotti P, Antunes MJ et al (2015) ESC Guidelines for the management of infective endocarditis: the Task Force for the Management of Infective Endocarditis of the European Society of Cardiology (ESC). Endorsed by: European Association for Cardio-Thoracic Surgery (EACTS), the European Association of Nuclear Medicine (EANM). Eur Heart J 2015;36:3075–3128.
77. Pelletier-Galarneau M, Abikhzer G, Harel F, Dilsizian V (2020) Detection of native and prosthetic valve endocarditis: incremental attributes of functional FDG PET/CT over morphologic imaging. Curr Cardiol Rep 22:93
78. Bruun NE, Habib G, Thuny F, Sogaard P (2014) Cardiac imaging in infectious endocarditis. Eur Heart J 35:624–632
79. Mahmood M, Kendi AT, Ajmal S et al (2019) Meta-analysis of 18F-FDG PET/CT in the diagnosis of infective endocarditis. J Nucl Cardiol 26:922–935
80. Gomes A, Glaudemans A, Touw DJ et al (2017) Diagnostic value of imaging in infective endocarditis: a systematic review. Lancet Infect Dis 17:e1–e14
81. Philip M, Tessonnier L, Mancini J et al (2019) 333018F-fluorodeoxyglucose positron emission tomography computed tomography (PET/CT) for the diagnosis of prosthetic valve infective endocarditis (PVIE): a prospective multicenter study [abstract]. Eur Heart J 2019;40:ehz745.0082.
82. de Camargo RA, Sommer Bitencourt M, Meneghetti JC et al (2020) The role of 18F-fluorodeoxyglucose positron emission tomography/computed tomography in the diagnosis of left-sided endocarditis: native vs prosthetic valves endocarditis. Clin Infect Dis 70:583–594
83. Mahmood M, Abu SO (2020) The role of 18-F FDG PET/CT in imaging of endocarditis and cardiac device infections. Semin Nucl Med 50:319–330
84. Blomström-Lundqvist C, Traykov V, Erba PA et al (2020) European Heart Rhythm Association (EHRA) international consensus document on how to prevent, diagnose, and treat cardiac implantable electronic device infections-endorsed by the Heart Rhythm Society (HRS), the Asia Pacific Heart Rhythm Society (APHRS), the Latin American Heart Rhythm Society (LAHRS), International Society for Cardiovascular Infectious Diseases (ISCVID) and the European Society of Clinical Microbiology and Infectious Diseases (ESCMID) in collaboration with the European Association for Cardio-Thoracic Surgery (EACTS). Europace 22:515–549
85. Vilacosta I, Sarria C, San Roman JA et al (1994) Usefulness of transesophageal echocardiography for diagnosis of infected transvenous permanent pacemakers. Circulation 89:2684–2687
86. Rubini G, Ferrari C, Carretta D et al (2020) Usefulness of ^{18}F-FDG PET/CT in patients with cardiac implantable electronic device suspected of late infection. J Clin Med 9:2246
87. Sarrazin JF, Philippon F, Tessier M et al (2012) Usefulness of fluorine-18 positron emission tomography/computed tomography for identification of cardiovascular implantable electronic device infections. J Am Coll Cardiol 59:1616–1625
88. Graziosi M, Nanni C, Lorenzini M et al (2014) Role of ^{18}F-FDG PET/CT in the diagnosis of infective endocarditis in patients with an implanted cardiac device: a prospective study. Eur J Nucl Med Mol Imaging 41:1617–1623
89. Ploux S, Riviere A, Amraoui S et al (2011) Positron emission tomography in patients with suspected pacing system infections may play a critical role in difficult cases. Heart Rhythm 8:1478–1481
90. Mahmood M, Kendi AT, Farid S et al (2019) Role of ^{18}F-FDG PET/CT in the diagnosis of cardiovascular implantable electronic device infections: a meta-analysis. J Nucl Cardiol 26:958–970
91. Diemberger I, Bonfiglioli R, Martignani C et al (2019) Contribution of PET imaging to mortality risk stratification in candidates to lead extraction for pacemaker or defibrillator infection: a prospective single center study. Eur J Nucl Med Mol Imaging 46:194–205
92. Kim J, Feller ED, Chen W, Liang Y, Dilsizian V (2019) FDG PET/CT for early detection and localization of left ventricular assist device infection: impact on patient management and outcome. JACC Cardiovasc Imaging 12:722–729
93. de Vaugelade C, Mesguich C, Nubret K et al (2019) Infections in patients using ventricular-assist devices: comparison of the diagnostic performance of ^{18}F-FDG PET/CT scan and leucocyte-labeled scintigraphy. J Nucl Cardiol 26:42–55
94. Okeie K, Shimizu M, Yoshio H et al (2000) Left ventricular systolic dysfunction during exercise and dobutamine stress in patients with hypertrophic cardiomyopathy. J Am Coll Cardiol 36:856–863
95. Aoyama R, Takano H, Kobayashi Y et al (2017) Evaluation of myocardial glucose metabolism in hypertrophic cardiomyopathy using 18F-fluorodeoxyglucose positron emission tomography. PLoS ONE 12:e0188479
96. Tzolos E, Andrews JP, Dweck MR (2020) Aortic valve stenosis-multimodality assessment with PET/CT and PET/MRI. Br J Radiol 93:20190688
97. Gupta K, Dixit P, Ananthasubramaniam K (2021) Cardiac PET in aortic stenosis: potential role in risk refinement? J Nucl Cardiol. https://doi.org/10.1007/s12350-021-02714-7
98. Zhou W, Bajaj N, Gupta A et al (2021) Coronary microvascular dysfunction, left ventricular remodeling, and clinical outcomes in aortic stenosis. J Nucl Cardiol 28:579–588
99. Dulgheru R, Pibarot P, Sengupta PP et al (2016) Multimodality imaging strategies for the assessment of aortic stenosis: viewpoint of the Heart Valve Clinic International Database (HAVEC) Group. Circ Cardiovasc Imaging 9:e004352